REPORT DOCUMENTATION PAGE

Form Approved
OMB No. 0704-01-0188

PLEASE DO NOT RETURN YOUR FORM TO THE ABOVE ADDRESS.

1. REPORT DATE *(DD-MM-YYYY)*	2. REPORT TYPE	3. DATES COVERED *(From - To)*
20–10–2004	Final Report	

4. TITLE AND SUBTITLE

ADVANCED MODELING OF MIXED SIGNAL SYSTEMS

5a. CONTRACT NUMBER
N66001-01-1-8921

5b. GRANT NUMBER

5c. PROGRAM ELEMENT NUMBER

6. AUTHORS

M. Steer
North Carolina State University

5d. PROJECT NUMBER

5e. TASK NUMBER

5f. WORK UNIT NUMBER

7. PERFORMING ORGANIZATION NAME(S) AND ADDRESS(ES)

North Carolina State University
Raleigh, NC 27612

SSC San Diego
COTR: J. Rockway
San Diego, CA 92152-5001

8. PERFORMING ORGANIZATION REPORT NUMBER

9. SPONSORING/MONITORING AGENCY NAME(S) AND ADDRESS(ES)

Defense Adavanced Research Projects Agency
Defense Sciences Office
Arlington, VA 22203-1714

10. SPONSOR/MONITOR'S ACRONYM(S)
DARPA\DSO

11. SPONSOR/MONITOR'S REPORT NUMBER(S)

12. DISTRIBUTION/AVAILABILITY STATEMENT

Approved for public release; distribution is unlimited.

13. SUPPLEMENTARY NOTES

14. ABSTRACT

This final report describes software products produced in the Advance Modeling of Mixed Signal Systems project and outlines project accomplishments. Several software tools were developed and made available. The capability developments behind the tools were demonstrated in the transient simulation of a radar system, believed to be the first to require simulation with high dynamic range and arbitrary-length time delays. Benchmarks for the NeoCAD program were produced. Many aspects of the program were transferred into DoD-relevant commercial programs.

15. SUBJECT TERMS

Mission Area: Software Development
modeling
mixed signal X-band radar
dynamic range
radar
technology transfer
time delays

16. SECURITY CLASSIFICATION OF:			17. LIMITATION OF ABSTRACT	18. NUMBER OF PAGES	19a. NAME OF RESPONSIBLE PERSON
a. REPORT	b. ABSTRACT	c. THIS PAGE			C. Hanson
U	U	U	UU	64	19B. TELEPHONE NUMBER *(Include area code)* (619) 553-5242/2164

February 2005

Advanced Modeling of Mixed Signal Systems

M. Steer
North Carolina State University

SSC San Diego

TABLE OF CONTENTS

1 SUMMARY OF ACCOMPLISHMENTS

1.1 Characteristics of Program

First ever demonstration of military critical capabilities:

- High dynamic range transient simulation
- First full-wave interconnect Modeling Tool
- Only way to model critical technologies
- Molecular electronics
- Tunneling in nanoelectronics
- Radar systems (transient)
- Driver of commercial developments
- Open Source

1.2 Software tools

We have developed five software packages responding to feedback from users.

These packages are:

- fREEDA
    - High dynamic range multi physics simulator
    - Easy development of advanced device models
    - Many device models never before implemented
- S2IBIS3 (Spice To IBIS)
    - Automated digital macromodeling tool
- EMPDK

- EM-Aware physical design kit tool (JAVA)

- UIUC2D
  - EM modeling tool for 2D geometries
- ICWAVE
  - On chip, comprehensive, 3D EM modeling
  - Technology used in part in NeoRF (NeoLinear)
- PRIME
  - EM Reduced Order Model interconnect modeler
  - Directly interfaces with fREEDA
  - Synthesizes R, L, C, K models for Spice.

All packages can be accessed through http://www.freeda.org

PRIME and UIUC2D http://alpha1.ece.uiuc.edu/download

For PRIME: username: prime pwd: fitting

For UIUC2D: username: uiuc2d pwd: rlcgsyn

For ICWAVE Contact Andreas Cangellaris

We will continue to maintain these products.

1.3 Modeling of Mixed Signal X-Band Radar

Traditional microwave subsystem design is based on harmonic balance (frequency-domain) simulations. However real-world effects due to transients, e.g. temperature during pulsed

Transmission are not captured. Many effects are signal dependent and the chirp-like radar signal cannot be represented in the frequency domain. Only a transient simulation will capture all effects but the problem here is that transient simulation has typically low dynamic range and the undesirable effects such as spectral regrowth cannot be seen. Many of the developments required to develop a transient simulator with all of the attributed required for circuit-level radar simulation are described in subsequent sections.

The canonical radar transmit system shown in Figure 1 was modeled. The mixer was considered to be ideal but a high order bandpass filter, a circuit-level model of an X-band MMIC, and a behavioral model of a Traveling Wave Tube Amplifier (TWTA) were modeled. The TWTA model requires long time delays that have never been modeled in a transient simulator previously.

Figure 2 shows the transient waveform at the output of the TWTA. The initial spike results from turning the system on. This is clearly an effect that must be suppressed and its level could not be determined in a traditional harmonic balance simulation. The spectrum at the output is shown in Figure 3. It was not possible to use an FFT to arrive at this spectrum with this fidelity. Instead first principles Fourier transformation was used. We believe that these results are the first circuit-level transient simulation of a radar. We are currently constructing this radar but comparisons between simulations and measurements are not available for this report. Note that actual bandpass filter, driver amplifier and TWTA were modeled and models of the individual subsystems have been experimentally verified.

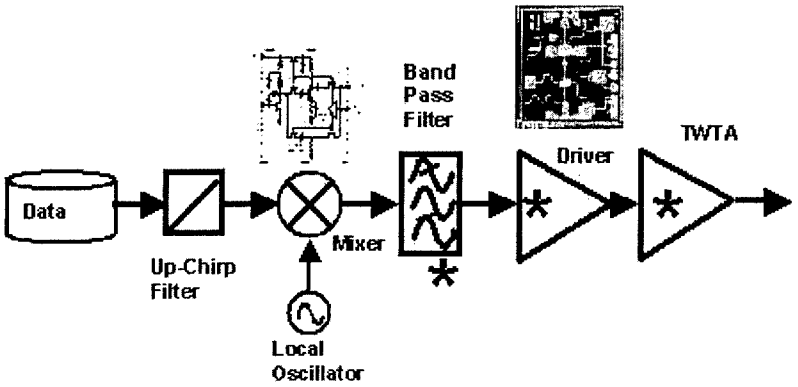

Figure 1. An X-band radar transmitter.

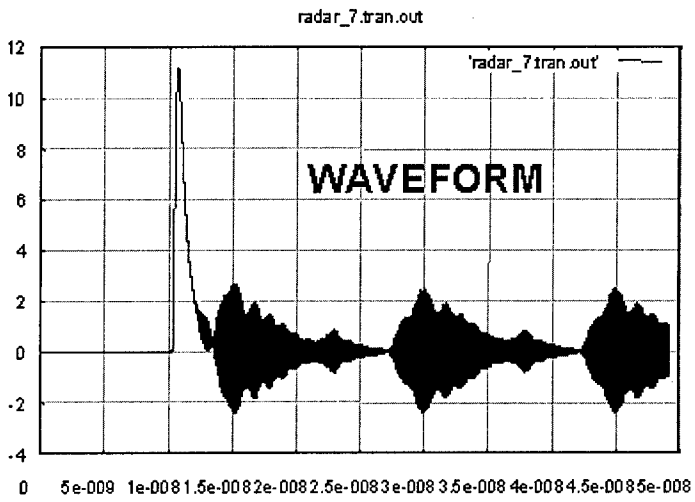

Figure 2. Transient waveform at the output of the TWTA.

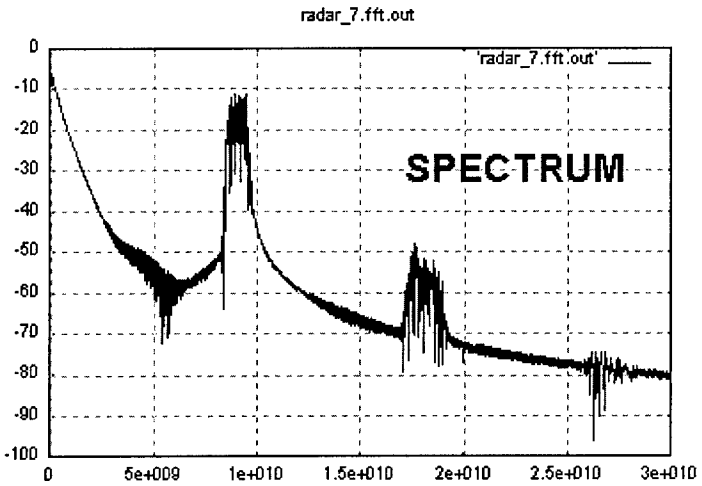

Figure 3. Spectrum at the output of the TWTA.

1.4 Multi Physics Capability

fREEDA is the only simulator with advanced device models capturing full physics. Examples are models of tunneling in:

- Tunnel Diode
- MOSCAP, See Figure 4
- TFT
- Molecular Diode, See Figure 5

The tunnel process cannot be expressed as a current-charge-voltage expression. We must use state variables to implement tunneling correctly. In addition fREEDA is the only simulator that can handle long time delays of more than 2 or 3 time steps. Figure 6 shows the input and output waveforms of the X-band TWTA.

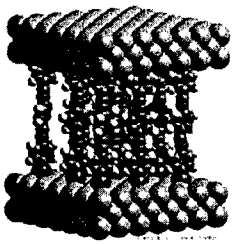

Figure 4. Molecular Electronics

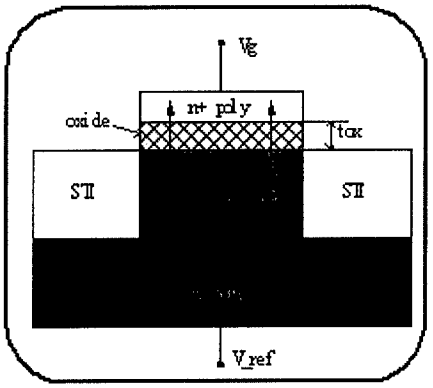

Figure 5. MOSCAP

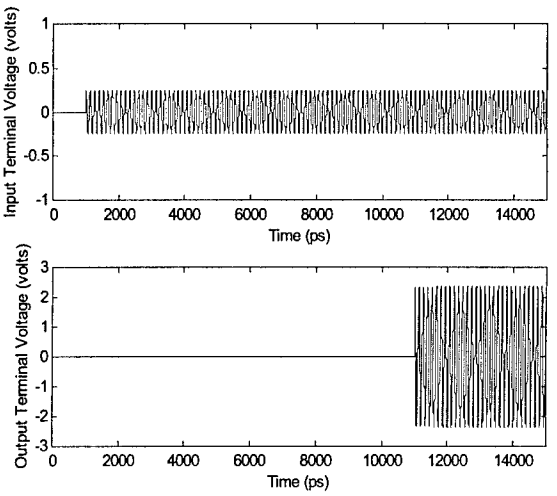

Figure 6. Input and output waveforms of the TWTA demonstrating the ability to model long time delays.

1.6 Benchmark Data

NeoCAD benchmark data (microwave measurements) developed in first year of NeoCAD. Used by EM modeling groups to validate data and used in several NeoCAD publications. Only measured on-chip benchmark characterizations openly available. The three main categories of devices benchmarked are sown in Figures 7, 8 and 9.

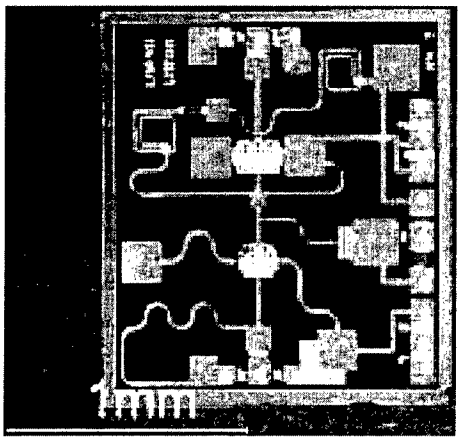

Figure 7. X-Band MMIC

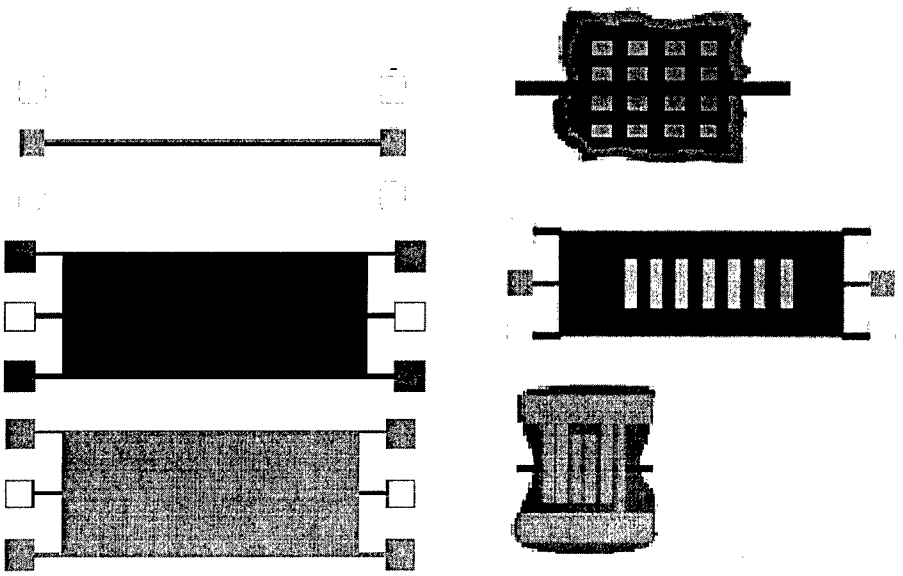

(a) (b)

Figure 8. Silicon interconnect characterization (0.25 Micron).

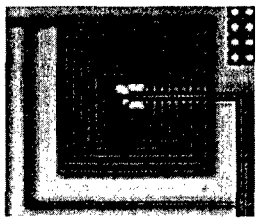

Figure 9. Coupled Inductor (0.25 micron).

1.7 NCSU/NeoCAD Technology Transfer

fREEDA (multiphysics circuit simulator)

- Open source, anyone can study technology.
- A PhD graduate of the program moved to Synopysis where he led part of the technical development of their latest simulator based in part on fREEDA Technology.
- A senior executive at Agilent told me that fREEDA technology has been implemented in their ADS simulator.
- A developer at Cadence Design Systems has indicated that fREEDA has been studied extensively in the Spectre group at Cadence.

ICWAVE (Full wave on-chip EM simulator)

- Vladimir Okhmatovski, PostDoc Univ. Illinois, moved to NeoLinear and worked on the development of NeoRF partly incorporating ICWAVE Technology

S2IBIS (Automated digital macromodel tool)

- Extremely successful, major reason IBIS macromodels have been successful.
- Widely used: 10 downloads per day. Support provided by EIA consortium. Used by virtually all IC vendors. Impacted possibly every military electronic systems

EM-PDK

- EM-Aware Physical Design Kit
- Used by several NeoCAD groups to process interconnect data.

The role of a university in computer aided engineering is to show what is possible and facilitate the transfer of tools and know-how to commercial CAD companies. The most successful method of transfer is students transferring to companies.

2 Details on fREEDA Development

2.1 fREEDA VERSUS SPICE

1. fREEDA is a multi physics simulator
    (a) It can dó things that cannot be done any other way.
    (b) High transient dynamic range.
    (c) Mixed physics; Long time steps; Rapid model development.
    (d) Mixed Electro / Thermal / EM
    (e) Many first open source implementations of models.
    (f) Advanced concepts, automatic differentiation, general purpose.
    (g) Serves as a demonstration of what can be done.
    (h) As open source it is being copied and concepts utilized by many companies.
2. HOWEVER, it is not a Spice replacement.
    (a) E.G. Spice and fREEDA solve a nonlinear problem differently.
    (b) If the device model is not physically consistent then different solvers will give different results. (This is the case with BSIM models)
    (c) Works for all other models. (e.g. EKV)

2.2 Time Step Development

A major technology that limits the dynamic range of a circuit simulator is the choice of time step and the associated estimate of error. A transient simulator must estimate its error at each time step and adjust its time point selection accordingly. In Spice the algorithm is to compare the nonlinear solution to a linear projection from the solution at the last time point. One side effect

of this is that the time step shrinks as the derivative of a waveform changes sign, for example over the top of a sinewave. More time points than are needed lead to additional numerical noise. The other fact is that there is a better way to estimate error. In fREEDA two different nonlinear solutions are performed and these are compared, see Figure 10. This is a much better estimate of error especially "over the top of a sinewave." The result is that a better time step is used and higher dynamic range.

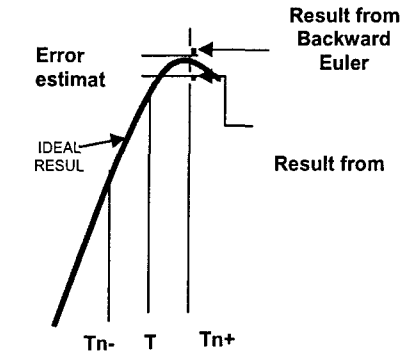

(a)

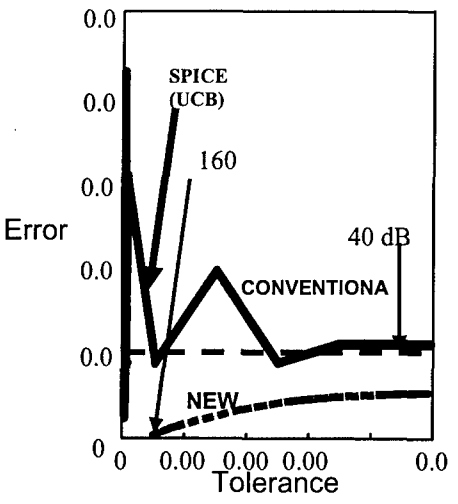

(b)

Figure 10. Estimation of error in fREEDA: (a) time point selection; and (b) effect of specification of tolerance on error.

2.3 Validation of dynamic range

Various definitions could be used for the dynamic range of a simulator. The bets definition to be used should be based on the types of signals to be captured. In the NeoCAD project we proposed the adoption of the metric of the smallest detectable signal (a single frequency tone) in the presence of a tone close in frequency. This metric was adopted by others in the NeoCAD community. Data supporting our claim is shown in Figure 11. In Figure 11(a) is the layout view of a High Dynamic Range PHEMT 2-stage Low Noise Amplifier MMIC operating from 8.5 GHz to 14 GHz with 18dB Gain. It has a +6 V Supply Voltage, 2 dB Noise Figure. It is used as a pre-driver amplifier for European phased array radar as well as commercial communications applications. Figure 11(b) shows measured two tone data compared to measurements obtained with fREEDA transient analysis and Agilent ADS' harmonic balance analysis. Note that in transient analysis we can obtain higher dynamic range than obtainable in the industry's leading commercial harmonic balance simulator. One hallmark of the work that we do is comparison with measurements wherever possible.

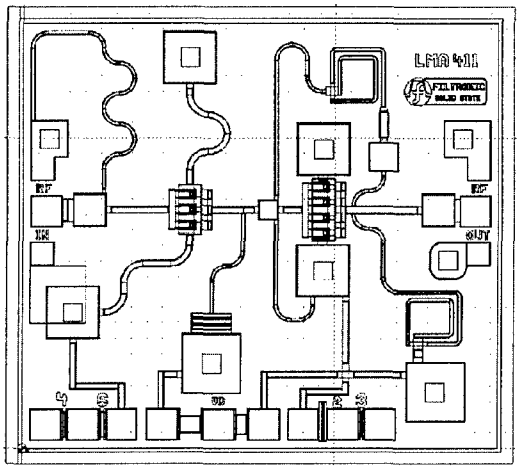

(a)

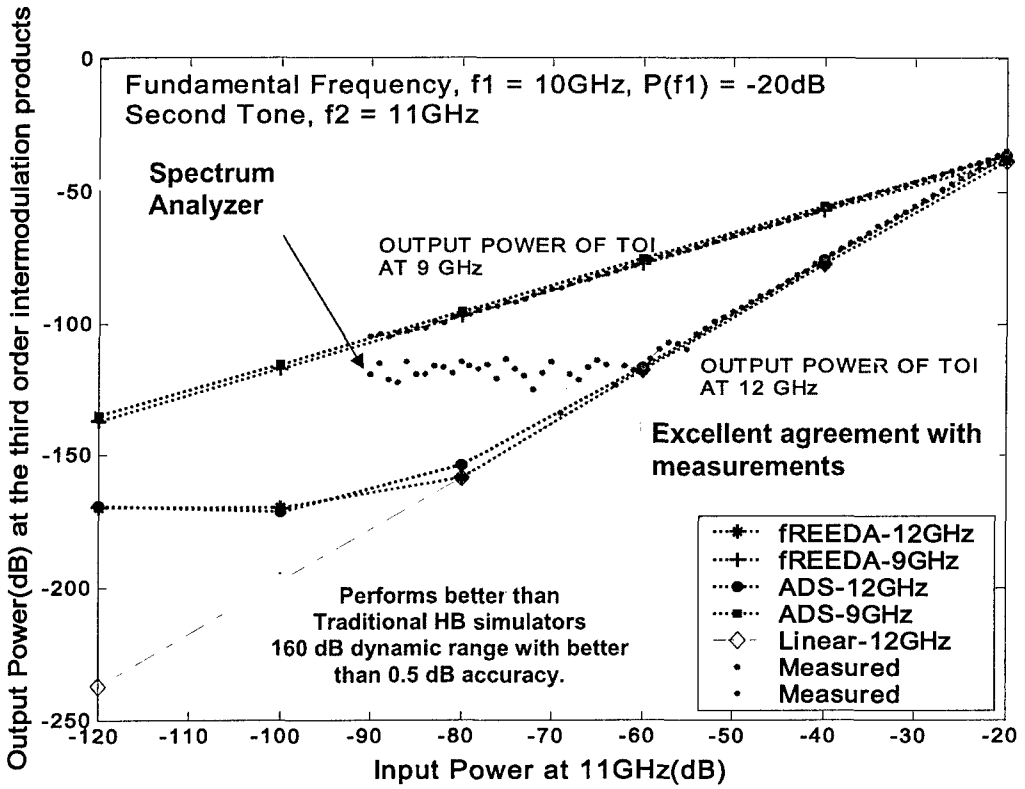

(b)

Figure 11. Measured and simulated results for an X-band MMIC: (a) MMIC; and (b) simulation results.

2.4 Electromagnetic Development

2.4.1 Electromagnetic Aware Physical Design Kit (EM-PDK)

EM-PDK (Java) is both a stand alone program and integrated into Electric. Electric is a GNU-licensed IC design tool. We have integrated EM-PDK into Electric and is distributed as part of Electric. It is written in the Java language and operates in two distinct modes:

- Stand alone mode:
    - Parses a layout file and extracts electromagnetic (EM) features that are important in electromagnetic analysis, it is EM aware.
    - Creates cif output. (Metals, dielectrics thicknesses and properties only).
    - Pass to electromagnetic simulator simulator.
- Electric mode
    - identifies local reference groups and assigns local
    - reference terminals. Assigns terminal numbers.
    - creates spice file + em-aware layout file

In the Electric mode a tool flow using EM-PDK is shown in Figure 12.

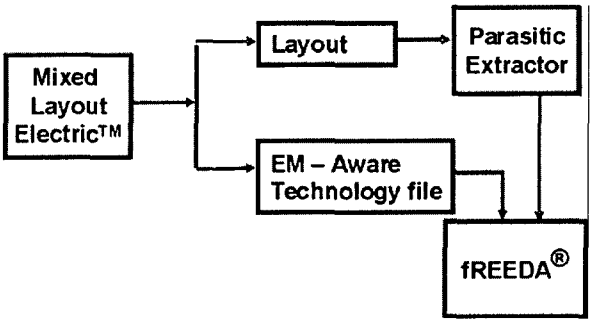

Figure 12. Integrating fREEDA and Electric usin EM-PDK.

2.4.2 Modifications to Electric Editor

Electric Editor (or known simply as Electric) is a powerful layout tool that is GNU-licensed. It is widely used. It handles MOS-Bipolar transistors, MOS-Bipolar Schematics, and HDLs. It has a common Layout-Schematic Interface, see Figure 13. It supports various interface standards including CIF, GDS II, VHDL, Verilog. NCSU made a number of modifications to include naming of nodes at points of connection between schematic and layout; support for materials properties added (Layer Thickness; Loss Tangent; and Dielectric Constant) All modifications have been included in the current Electric Editor release.

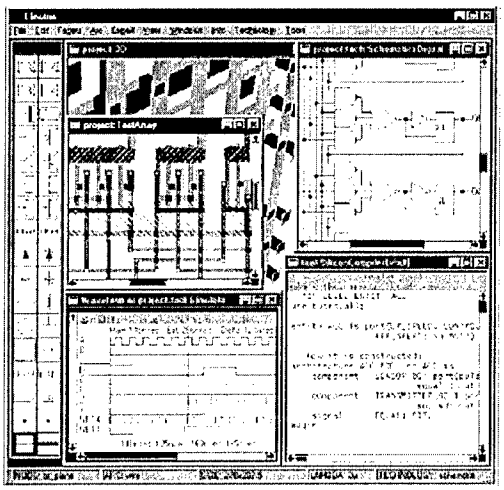

Figure 13. Screen Capture of Electric.

2.5 IBIS Macromodeling Development

IBIS is a behavioral macromodeling language that has been widely adopted by industry, see http://www.eia.org/eig/ibis/ibis.htm . The structure of the model is shown in Figure 14. One

reason why this model has been so successful is the availability of an automatic macromodel generation tool. This tool is S2IBIS (Spice-to-IBIS). The development of version 3 of the tool, S2IBIS3, was supported by NeoCAD. S2IBIS3 is being downloaded from the NCSU website at the rate of 10 per day currently. Brief highlights are

- Spice To IBIS Macromodel Converter
- Supports HSpice & Spice3
- Written in Java (platform independent) Tested Windows, Unix, Linux
- Provides heuristic convergence assistance.
- More than 1,000 downloads since 2/1/2004. (Now 10 per day)
- Version 3 good for 2 GHz digital systems
- IBIS model in fREEDA (first as open source)

IBIS is a notoriously difficult model to implement in a simulator and there are only a few implementations in Spice. By providing an open source implementation we have told the world how to implement the model.

At the start of NeoCAD the start-of-the-art was S2IBIS2 the development of which was also supported by DARPA. S2IBIS2 was released 1996 and was written in the C, bison, perl languages. This resulted in platform portability problems and also problems assosicted with operating system upgrades. S2INIS2 could develop models that were good to 300 MHz

S2IBIS3 is compliant with IBIS3, version 3 of the IBIS spec. It is written in JAVA and so it is platform independent. It was tested by the EIA/IBIS group of companies including mentor graphics and cadence. S2IBIS3 supports Version 3 of the IBIS specification and is good to 2

GHz. Today almost no printed circuit board system or module can be designed without IBIS models of ICs.

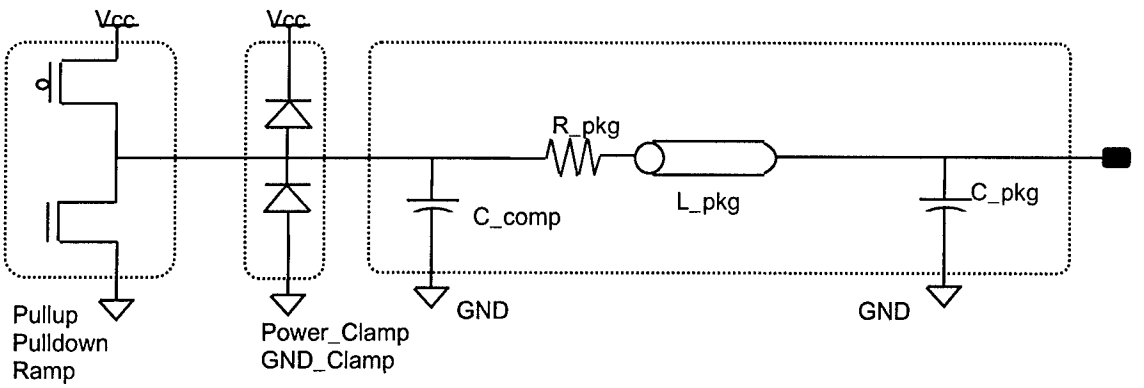

Figure 14. The IBIS model of a driver.

Nearly every semiconductor vendor uses S2IBIS to generate IBIS models that are generally made available on vendor websites. There are at least 300 vendors. Some of these are shown in Figure 15.

Actel
Aeroflex UTMC
Agere Systems
Agilent Technologies
Alchemy Semiconductor
Altera
AMCC (Applied Micro Circuits)
Advanced Micro Devices Inc (AMD)
AMI Semiconductor (AMIS)
American Microsystems
Analog Devices
Aptos Semiconductor
Asiliant
ATI Technologies
Atmel Corporation
Broadcom
Catalyst Semiconductor
Cicada Semiconductor
Cirrus Logic
Clear Logic
Conexant
Cypress Semiconductor
Dallas Semiconductor
Elantec
Elpida Memory, Inc.
Enhanced Memory Systems, Inc.
Exar

Fairchild Semiconductor
Fujitsu
Galileo Technology
GalvanTech
GSI Technology
Hewlett-Packard Company
HIFN
Hitachi Semiconductor
Hynix Semiconductor
Hyundai Electronics
IBM Microelectronics
I-Cube
IC Works
Infineon Technologies AG
Integrated Circuit Systems (ICS)
Integrated Device Technology (IDT)
Intersil
Intel
International Microelectronics, Inc. (IMI)
Integrated Silicon Solutions, Inc. (ISSI)
Intersil
Lattice Semiconductor Corporation (LTC)
Level 1 Communications
LSI Logic
Lucent Technologies
Marvell Technology Group, Ltd.

Maxim Integrated Products
Micrel Semiconductor
Micron Technology
Mindspeed Technologies
Mitel
Mitsubishi Semiconductors
MMC Networks
Mosel Vitelic
Motorola Semiconductor Products
MUSIC Semiconductors
Nanya Technology Corp.
National Semiconductor
NEC Electronics
On Semiconductor
Oxford Semiconductor
Pericom Semiconductor
Philips Semiconductor Logic
PLX Technology
PMC-Sierra
Quality Semiconductor
QuickLogic Corp.
Raltron
Ramtron
Samsung Semiconductor
Semtech
ServerWorks
SiberCore

Siemens AG
Silicon Storage Technology (SST)
Smart Modular Technologies
SMSC (Standard Microsystems Corp.)
Sony Electronics
STMicroelectronics
Texas Instruments
Toshiba
TranSwitch
TriQuint
Tundra Semiconductor
UTMC
VIA Technologies
Vitesse
White Electronic
Designs
Winbond
WooSung
Semiconductor
Xilinx
Zarlink Semiconductor
ZMD
Zentrum Mikroelektronik

+ hundreds more internal efforts

Figure 15. S2IBIS Semiconductor vendor users.

We have received hundreds of testimonials regarding S2IBIS (not always in the best English). Here are a few:

- Hello, my name is Albert Kim. I am DRAM engineer in Korea.

  I would like to say "Thank you for your s2ibis3".

  Thanks to your tool, I could save my time.

- "Great work has been done, thank you and good luck" - Christophe Robichon (Atmel)
- "Toshiba appreciates what you are doing!!" - Doran David (Toshiba)
- "Thank you for providing s2ibis3." - Bob Weppler (Rockwell)

We also undertook studies to a certain the accuracy of the IBIS model produced. Figure 16. Compares the simulated results using Spice netlist and an IBIS for an off-chip driver.

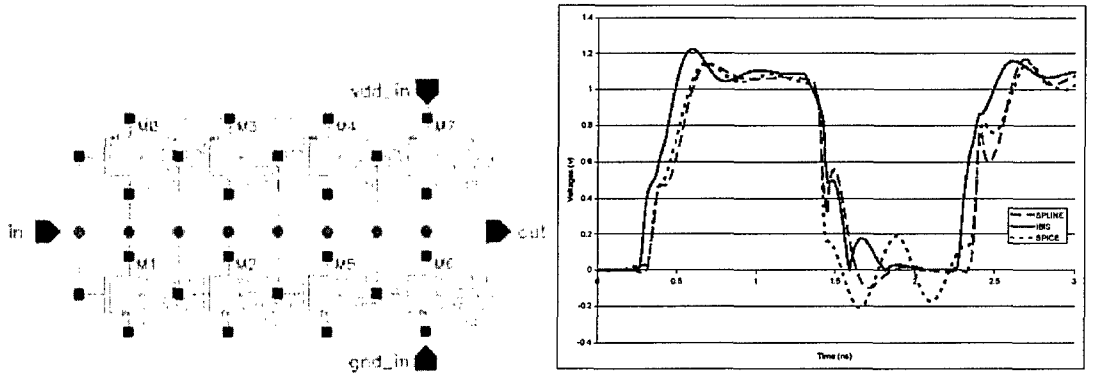

(a) (b)

Figure 16. Comparison of circuit level model and IBIS model: (a) an 8 inverter IC off-chip driver; and (b) comparison.

2.6 Advanced Device Modeling

In fREEDA many devices have been modeled for the first time. Several classes of models were developed and much work was put into modeling types of effects for the first time. One first was modeling the tunneling phenomenon is an extremely nonlinear process. A MOSCAP is one of devices that was modeled and a cross-section view is shown in Figure 17. This captures tunneling through a thin oxide layer which a particular problem in sub 100 nanometer transistors.

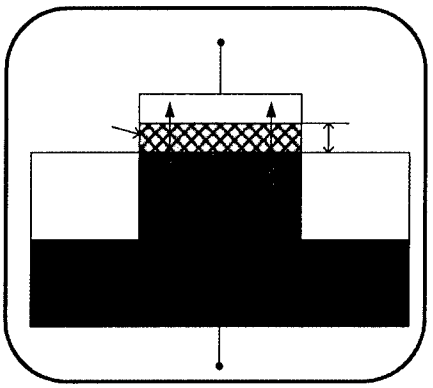

Figure 17. Cross-section of a MOSCAP that exhibits tunneling for thin oxide layers.

As is typical in modeling in fREEDA considerable effort goes into modeling effects for the first time. Once a phenomenon has been captured it can be replicated. In this case models were developed for Tunnel Diode, MOSCAP, TFT, and Molecular Diode which all exhibit similar tunneling. This is the first time these devices have ever been modeled in a simulator.

2.7 Molecular Device Modeling

Organic molecules exhibit a change in their equilibrium energy levels when biased such that current flows through them. Molecular device modeling is the modeling of this transport mechanism. It involves measuring and simulating the conductance characteristics of a nanopore. A nanopore consists of a few hundred to a thousand molecules sandwiched between two electrodes of a few nanometers width. Such a device has never been modeled in a simulator before and such modeling is essential in the development of molecular electronics. The molecular device modeled is shown in Figure 18 and the measured and modeled comparisons are shown in Figure 19.

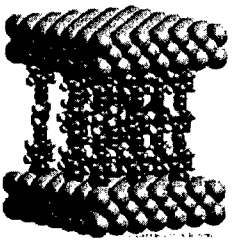

Figure 18. Molecular device model

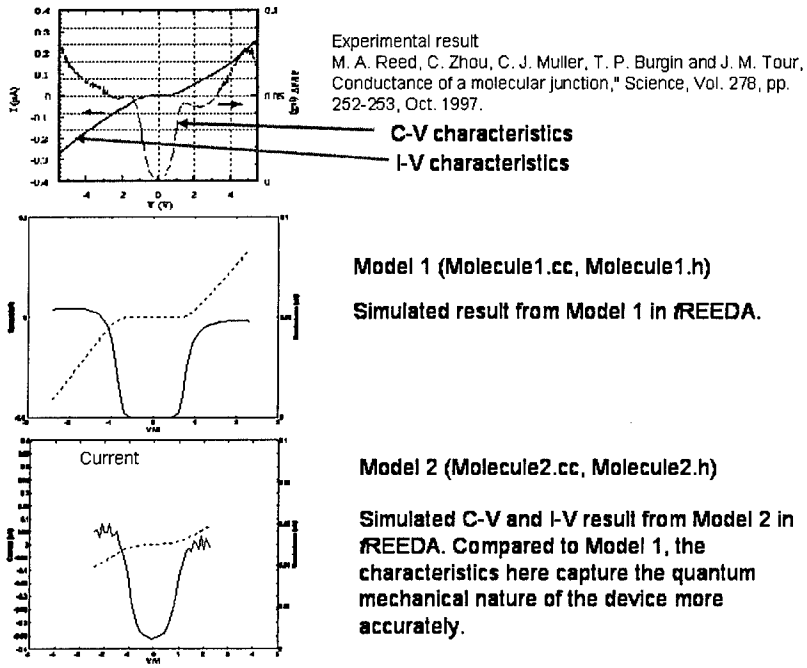

Figure 19. Simulated results for a molecular device.

The tunnel process inherent to molecular electronics cannot be expressed as a current-charge-voltage expression. We must use state variables to implement tunneling correctly.

2.8 Delay Modeling

Spice handles only short (< 4 time step) time delays using a polynomial interpolation model. fREEDA has no limit achieved through the implementation of an appropriate error measure. The response an indefinite time in the past is used as a state variable. This can only be implemented using a state variable based simulator. A TWT amplifier was used to validated fREEDA's ability to handle models with long time delays as shown in Figure 20. This feature has also been

implemented in many transistor models in fREEDA and so we model time delay in microwave transistors accurately.

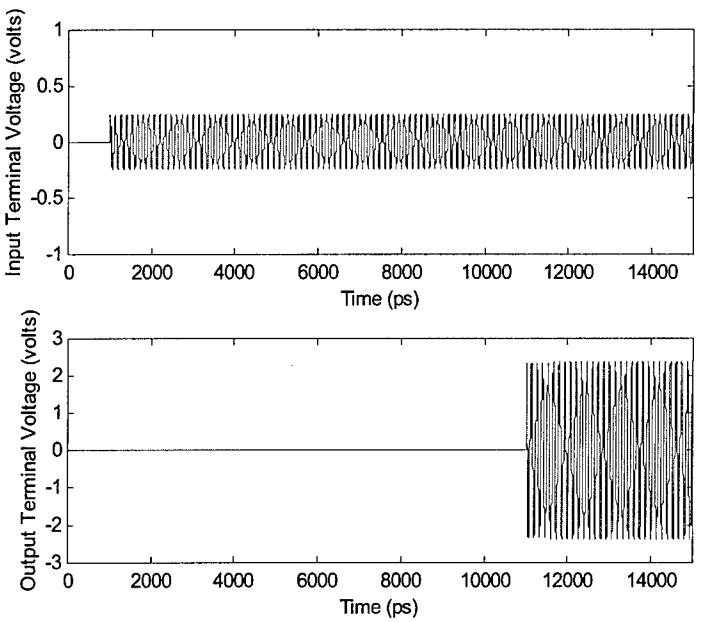

Figure 20. Demonstration of fREEDA's ability to model arbitrary time delays. Shown are the simulated input and out put responses of an X-band MMIC.

2.9 Details of Modeling of a an X-band radar system

The final demonstration of the capabilities of the tools that we developed were demonstrated using the simulation of a radar system. A radar signal is similar to that of an FM-chirped RF pulse. Using current tools it is not possible to model the nonlinear dynamics of this system. The design of the RF section of a radar currently utilizes frequency domain tools, specifically harmonic balance. A radar has high power transient signals that significantly affect operation.

The RF pulse can lead to spurious spectral emissions and result in transient heating effects. Capturing these effects in a transient simulation is not possible with current tools.

The attributes required to model a radar system with compromise are shown in Figure 21. At the start of the program there was limited ability to model the dynamic range of the radar system. An exception was using harmonic balance as in the ADS simulator but this simulator is not capable of capturing true radar effects. Since the program started both Spectre and ADS (with its inbuilt transient simulator) have improved their dynamic range in transient simulation. However they do not have the dynamic range of Spice. It is not clear exactly what their essential dynamic range as it appears that it is limited by their internal Fourier transform algorithm. For the fREEDA results presented here we used a special Fourier analysis. With fREEDA the dynamic range is 160 dB (to an accuracy of 0.5 dB). If we applied the same criteria to ADS and Spectre we could say that the range is limited to 120 dB. The attributes required all of the fREEDA developments mentioned previously.

As fREEDA is public domain any company can examine the code and determine how to achieve the same.

Feature	Initial State of The Art	Goal	Achieved
Dynamic Range	40–60 dB SPICE > 120 dB ADS	140 dB	160 dB
Multi Physics	Limited	Thermal / EM / Circuit	Thermal / EM / Circuit

Time Delay	2 or 3 time steps	Unlimited	Unlimited

Figure 21. Initial State of the Art, Goal and Achievement of fREEDA as used I transient radar system simulation.

While were unable to obtain models for all of the components of a radar system so we constructed one using available models of actual devices and idealized models. The radar system model considered is shown in Figure 22. It consists of a Linear FM Chirp source pulse modulated with center frequency 10 GHz and 100MHz bandwidth. It included the X-band Filtronic Solid State MMIC LNA, LMA 411 with 18dB gain (considered previously). The MMIC was followed by a Traveling Wave Tube (TWT). A circuit level model of the MMIC LNA was used and as seen previously simulations accurately capture measured data. The Bandpass Filter removes harmonic content from the MMIC output. Transient analysis of bandpass filters, especially narrow band bandpass filters is problematic. We have developed a technology based on Z-domain techniques that enables any order filter to be modeled in transient analysis. The TWT amplifier was model by a behavioral model using a novel behavioral model and based on measurements. One characteristic of the TWT amplifier is the very long time delays involved. Modeling this structure in fREEDA amounts to the first time a TWT has ever been modeled in a transient simulator. There are many firsts here and we will write journal papers up to cover all of these advances. Our primary objective recently has been to achieve the final phase milestones.

Various results are presented in Figures 23 through 29 for the transient waveforms and the spectra. The spectra observed could only be captured by first doing transient analysis. In Figure 22(b) missing features are indicated.

Radar Xmit System Block Diagram

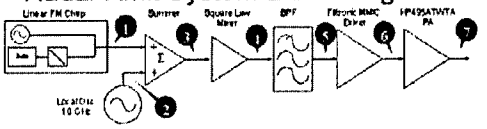

- Chirp Source: FM Linear downchirp from 1.5 to 0.5 GHz.
- LO Source: 10 GHz sine wave
- Summer and Square-Law mixer – both behavioral
- BPF: Z-domain cascade behavioral. -1 dB flat passband from 8.5 to 9.5 GHz, - 40 dB stopband edges at 8.25 and 9.75 GHz.
- Driver: Filtronic LMA411 MMIC ~18 dB gain (circuit model)
- PA: HP495A TWTA ~ 20 dB gain (behavioral)
- Output Signal: Linear FM Upchirped from 8.5-9.5 GHz.

(a)

Still To Do...

- White Noise source (based on gaussian random variable)
  - User-specified $\mathcal{N}_0$
  - To facilitate receiver modeling
  - Presently generating random variates, but not at correct power spectral density
- Channel Model
  - Time delay plus insertion point for white noise source model, to facilitate receiver modeling
- New – Chebychev Z-domain filter model
  - Based upon Butterworth model
  - Turnaround time to develop should be short

(b)

Figure 22. Canonical radar system: (a) model; and (b) features missing.

Linear FM Downchirp Source (1)

From 0 to 16 ns. Pulse repetition period is 15 ns, chirp is 10 ns.

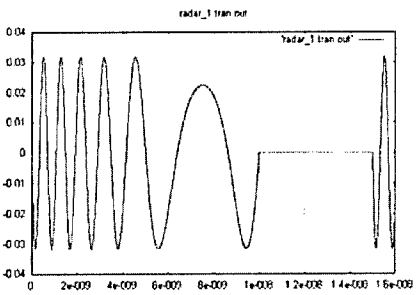

(a)

Linear FM Downchirp Source (1)

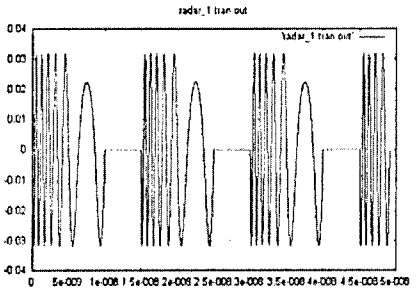

(b)

Figure 23. Waveforms at node (1): (a) short time; and (b) long time.

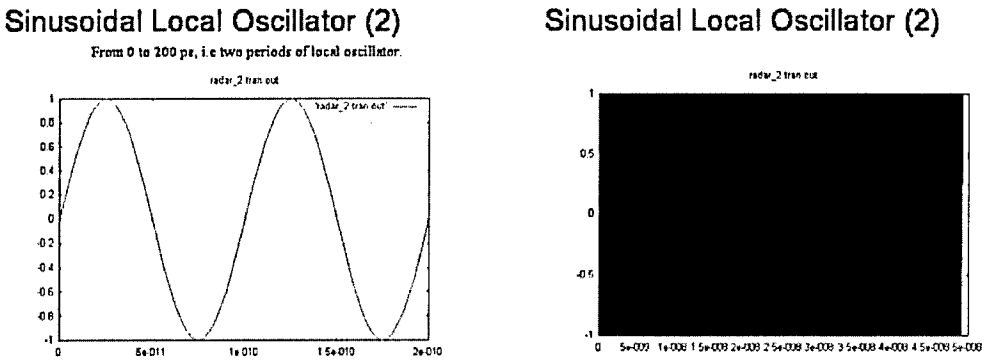

(a) (b)

Figure 24. Waveforms at node(2): (a) short time; and (b) long time.

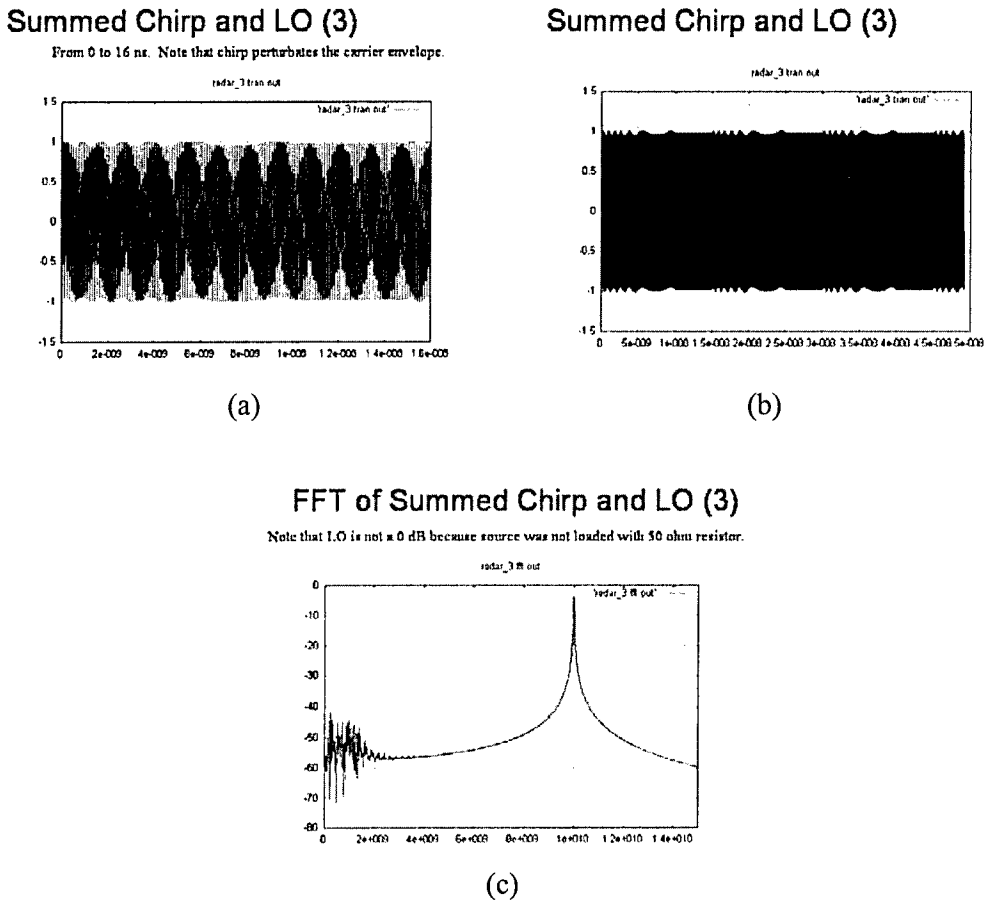

(a) (b)

(c)

Figure 25. Waveforms at node(3): (a) short time; (b) long time; and (c) spectrum.

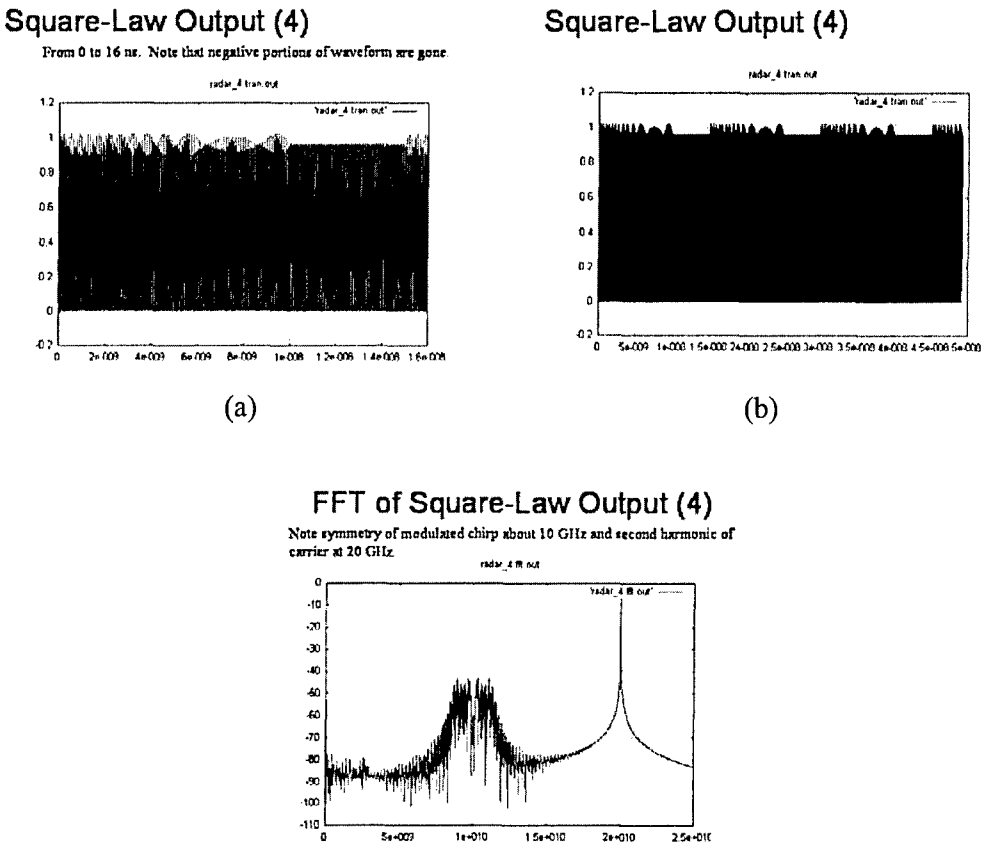

Figure 26. Waveforms at node(4): (a) short time; (b) long time; and (c) spectrum.

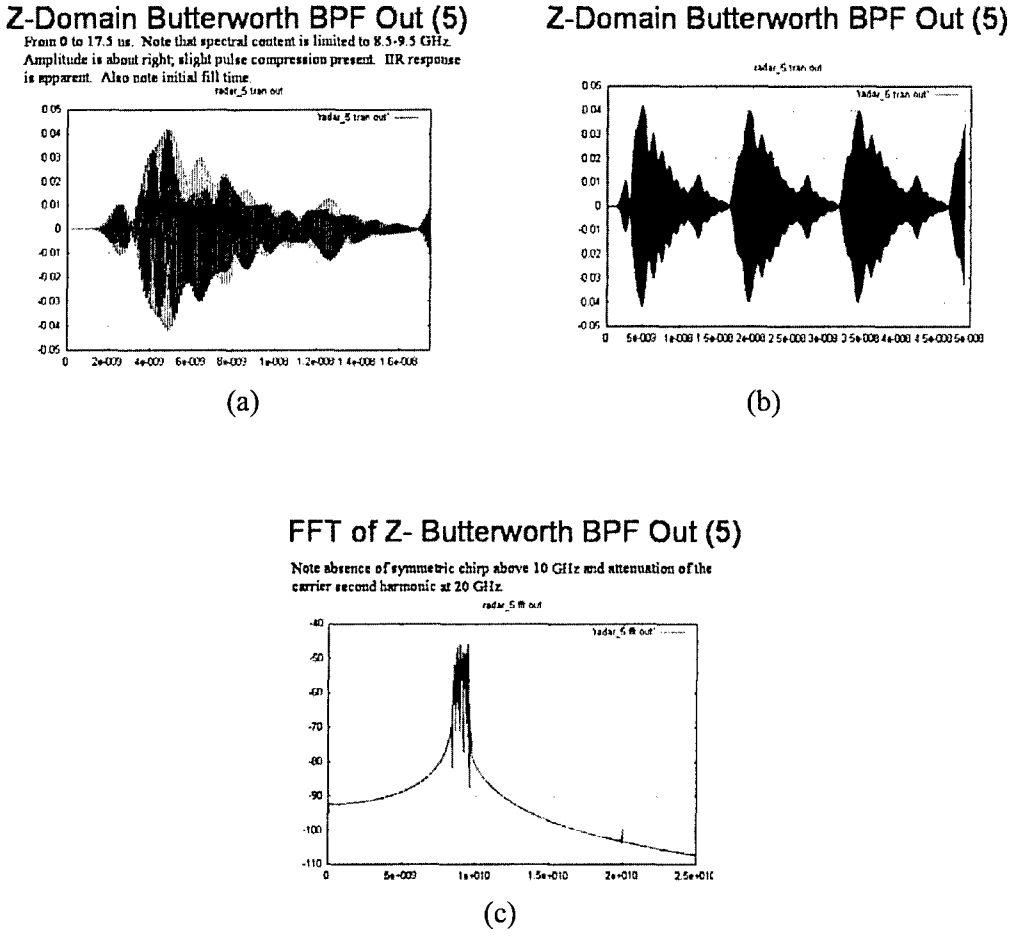

Figure 27. Waveforms at node (5): (a) short time; (b) long time; and (c) spectrum.

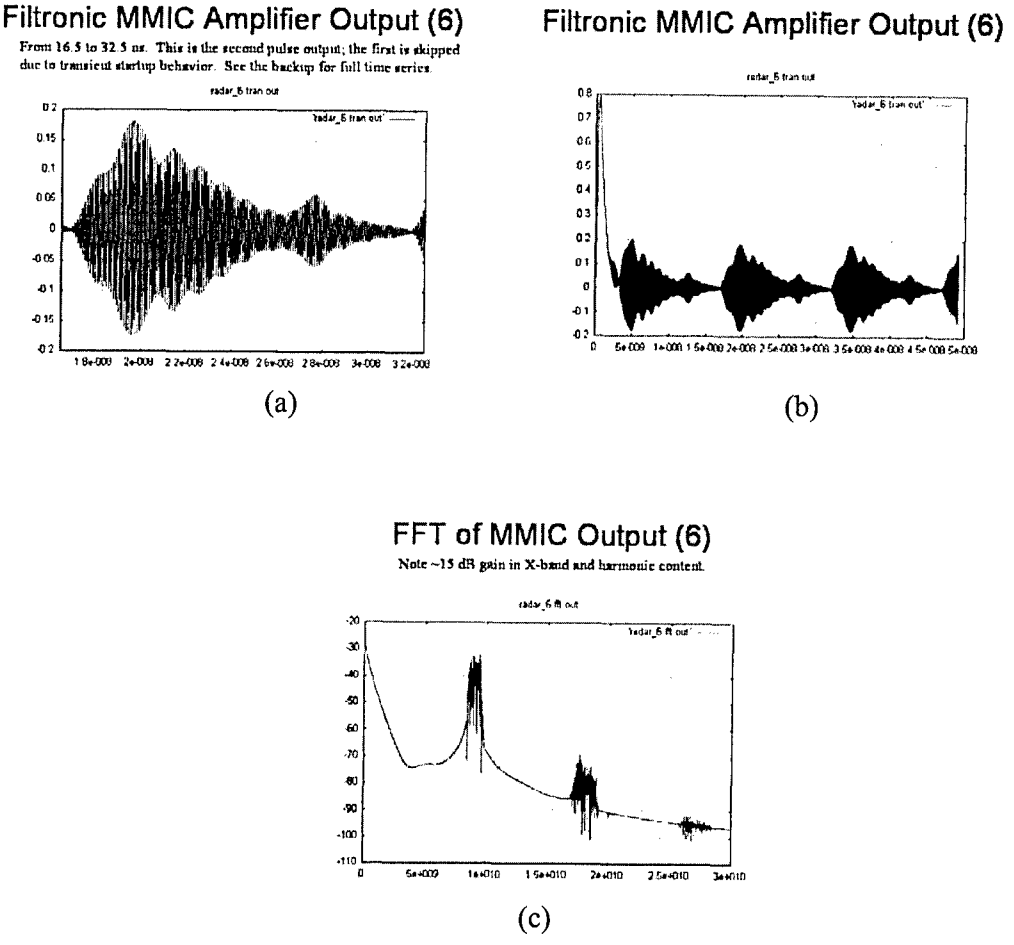

Figure 28. Waveforms at node (6): (a) short time; (b) long time; and (c) spectrum.

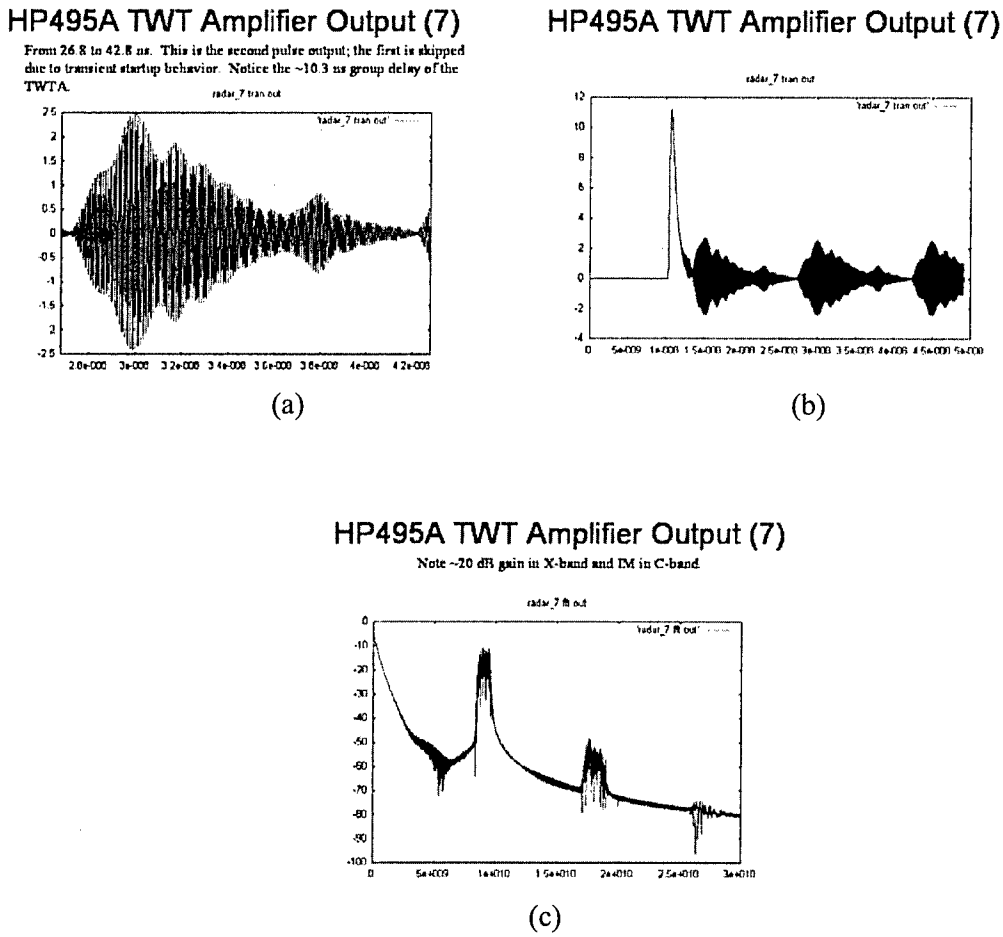

Figure 29. Waveforms at node (7): (a) short time; (b) long time; and (c) spectrum.

We are at the point where we can model any radar system at any level of accuracy. Our one big remaining problem is the implementation of a BSIM MOSFET model which is essential if we are to model the types of radar systems that Wright Patterson are interested in. Implementing a BSIM model was not in the initial scope of this project and has proven to be problematic. We are secured corporate funds to continue this part of the work.

3 Multigrid-Enhanced EM Modeling of the Power Grid On Chip

This EM modeling based on Maxwell equation using a finite volume model. The key attributes are:

- Model developed directly from physical structure
- Cumbersome and error-prone extraction of [L] and [C] avoided
- Rigorous modeling of electromagnetic effects
- In addition to power switching noise analysis it enables prediction of power grid-induced EMI between different blocks on the chip

The On-Chip Power Grid Transient Simulator combines:

- Electromagnetic rigor
- Comprehensive modeling
- Includes impact of semiconductor substrate
- SPICE Compatible. Initially we thought that we could only do this in fREEDA and although it is most efficiently done there we developed a scheme so tat it can be implemented in Spice.
- Direct implementation of SPICE models for non-linear drivers, decoupling caps, etc…
- Supports convenient interfacing with models for the off-chip power distribution network
- Supports both simultaneous switching noise and power grid-induced interference prediction

Results are documented in Figures 30 through 39.

FV-Based Modeling Methodology

Finite-volume discretization of Maxwell's equations

$$\oint_{C_F} \vec{E} \cdot d\vec{l} = -\frac{d}{dt} \iint_{S_F} \mu \vec{H} \cdot d\vec{S}$$

$$\oint_{C_A} \vec{H} \cdot d\vec{l} = \frac{d}{dt} \iint_{S_A} \varepsilon \vec{E} \cdot d\vec{S} + \iint_{S_A} \sigma \vec{E} \cdot d\vec{S}$$

- Micron-size cross-sectional dimensions and regular layout of the grid exploited to contain model complexity
  - Grid size of the order of grid feature size
  - Assignment of unknown electric & magnetic fields in space dictated by the electromagnetic effects that must be captured for accurate simulation
    - **Ohmic loss in the wires**
    - **Inductive effects during switching**
    - **Capacitive coupling and common impedance coupling for grid-induced interference calculation**

Figure 30 FM-based modeling methodology.

Implementation of Variable-Size Grid

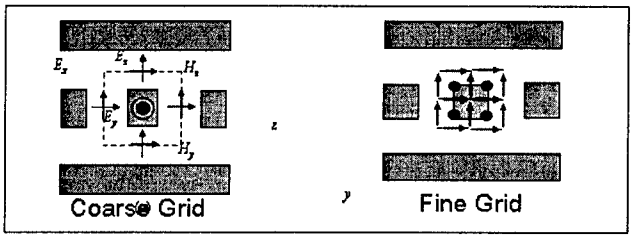

- The choice of grid coarseness is dependent on the simulation objective and the desired accuracy.
  - Switching noise simulation only: Coarse grid
  - Power grid-induced interference: Finer grid

Figure 31. Implementation of variable-size grid.

Compatibility with SPICE

The state-space form of the discrete model,

$$\begin{bmatrix} \mathbf{G} & \mathbf{D}_h \\ \mathbf{D}_e & \mathbf{R} \end{bmatrix} \begin{bmatrix} \mathbf{e} \\ \mathbf{h} \end{bmatrix} + \begin{bmatrix} \mathbf{C} & \mathbf{0} \\ \mathbf{0} & \mathbf{L} \end{bmatrix} \frac{d}{dt} \begin{bmatrix} \mathbf{e} \\ \mathbf{h} \end{bmatrix} = \begin{bmatrix} \mathbf{i}_S \\ \mathbf{v}_S \end{bmatrix}$$

is of the same form with the MNA formalism used in SPICE

Hence, it facilitates direct incorporation of lumped circuits and behavioral models for drivers and receivers

- **e , h : the discrete unknown fields**
- **G, R, L, C, D_h, D_e : sparse matrices (dependent on material and geometric properties of the structure)**
- **i_S, v_S : voltage & current sources connected to the grid**

Figure 32. Compatibility with Spice.

"Cartoon" of the On-Chip Grid

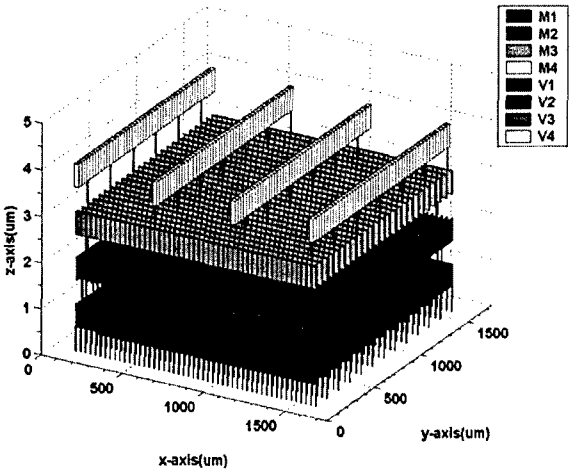

Figure 33. On-chip grid.

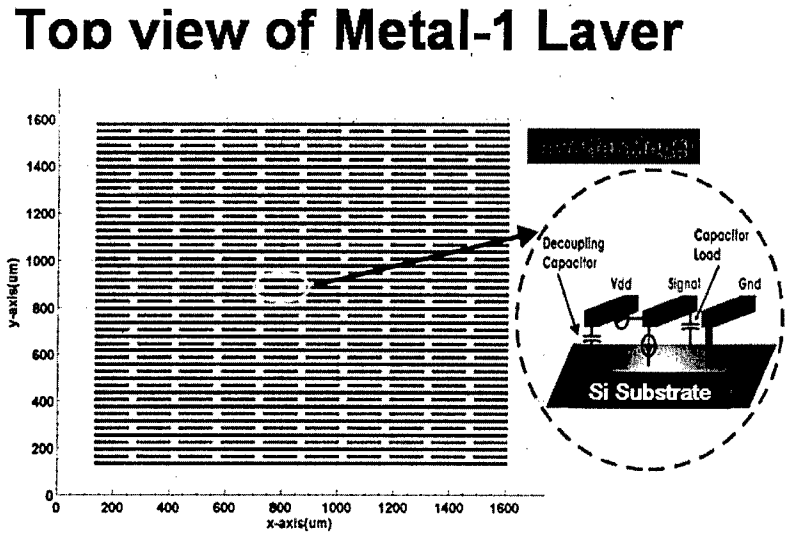

Figure 34. Metal-1 layer.

Additional Features of Solver

- Convenient interface to models for the off-chip power grid
  - Can be incorporated either in terms of SPICE net lists or in terms of a matrix rational function representation of their multi-port form
- Modeling of the semiconductor substrate
  - Effected through position- and frequency-dependent surface impedance relationships cast in terms of rational functions

Figure F. Features of solver.

Impact of semiconductor substrate on power grid switching response

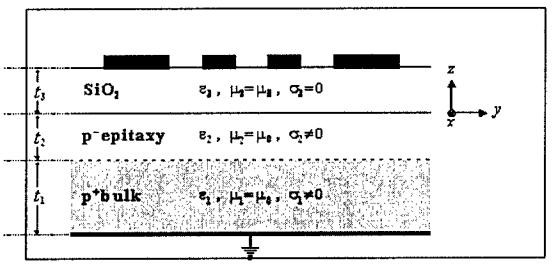

Case 0: Semiconductor substrate modeled as PEC
Case 1: t_1 = 198 μm, σ_1 = 104 S/m, t_2 = 2 μm, and σ_2 = 10 S/m
Case 2: t_1 = 200 μm, σ_1 = 104 S/m, t_2 = 0 (no epi)

Figure 36. Substrate impact.

Impact of semiconductor substrate…

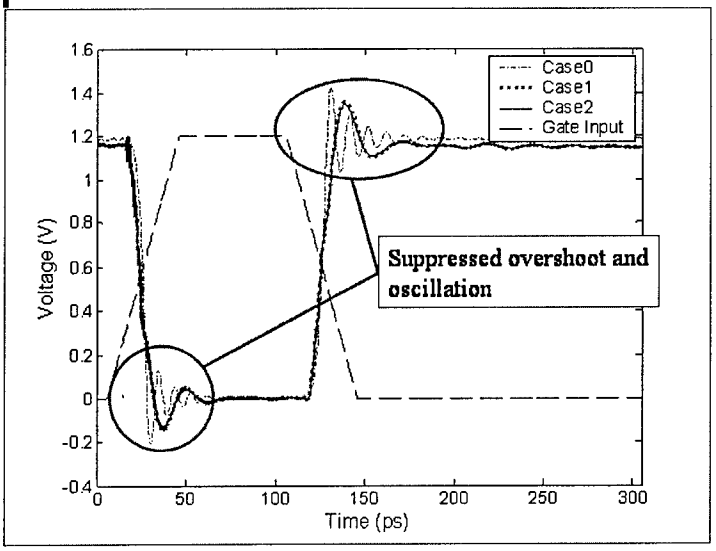

Figure 37. Substrate impact.

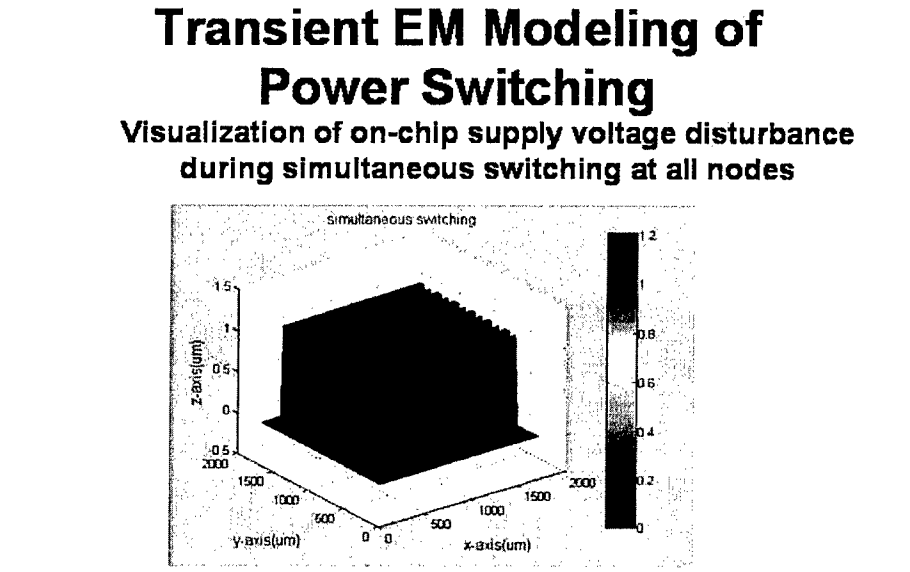

Figure 38. Model of power switching

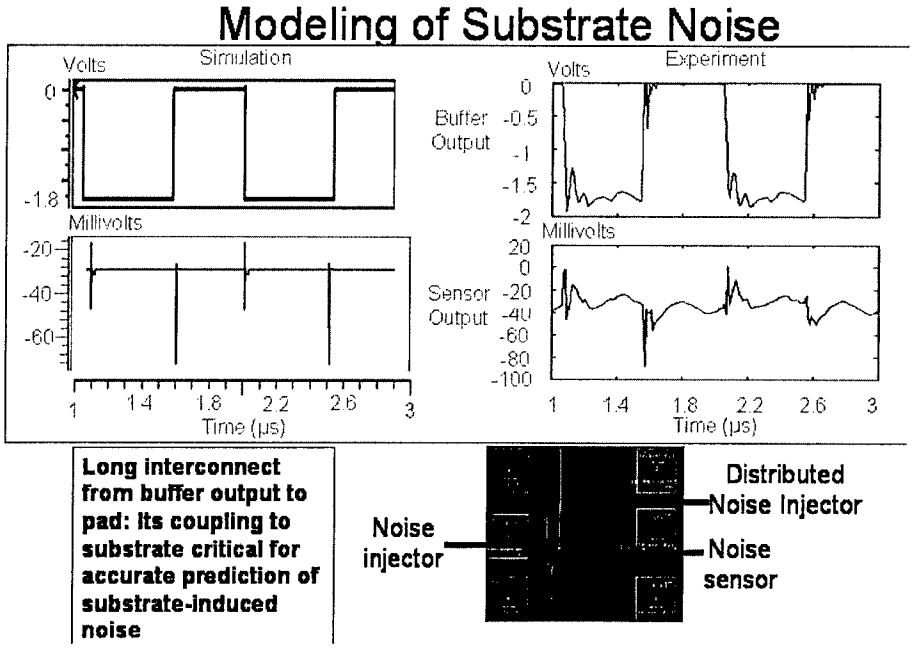

Figure 39. Model of substrate noise.

4 Opto-ElectronicModeling using fREEDA

4.1 Introduction

Progress in the field of opto-electronic device and optical component technology has led everyone to believe that optics can, practically, meet the bandwidth demand in future. Efforts are on to make all optical systems where most of the tasks e.g. switching, routing and amplification are done in optical domain. In spite of all these developments we still need drivers to turn on a laser and so we have a lot of electro-optical-thermal interactions taking place right at the point where light is actually generated. Further, when optical components and devices are put together in a system problems can arise because of the dispersive elements and feedback effects. So, before start fabricating the system one must study the electro-thermal-optical interactions and other optical effects such as feedback and effect of dispersion. To study such complex interactions one need a tool that can be used to simulate the system directly in terms of equations representing these interactions. Existing tools for OE system simulation involve either solving Maxwell equations using for example, the FDTD method that is computationally intensive or use equivalent circuits. Implementation of device models using an equivalent circuit approach has several drawbacks.

We have developed a new tool, fREEDA, capable of performing multi-physics simulations. fREEDA facilitates OE device modeling with sets of differential equations. This report is organized as follows. In first section, we discuss the validation of fREEDA for optoelectronic simulation using experiments and via comparison with other existing tools. Section II discusses the multimode VCSEL modeling using fREEDA. Next, we present the simulation results for free space optical system using fREEDA. Optical feedback effects and there impact on the system performance are discusses in the following section. Finally, we conclude with a summary of results and the future work.

4.2 fREEDA Validation

In this section, we discuss the validation of fREEDA for Vertical Cavity Surface Emitting Laser (VCSEL) modeling and simulation using the experiments and CFDRC physical VCSEL model. We also present the comparison of fREEDA results with the existing tools such as SPICE for package simulations.

We chose VCSEL for fREEDA validation as its optical properties depend strongly on the operating electrical and thermal conditions [2]. So, it makes the most suitable OE device for validating the multi-physics nature of fREEDA. Validation of fREEDA with the experiments and other simulators have been done in past[9,10]. We use the VCSEL model of Mena in our simulations and use the following rate equations [2]:

$$\frac{dN_0}{dt} = \frac{\eta_i I}{q} - \frac{N_0}{\tau_n} - \frac{G(N_0 - N_t)S}{(1+\epsilon S)} - \frac{I_l}{q} \tag{1}$$

$$\frac{dS}{dt} = -\frac{S}{\tau_p} + \frac{\beta N_0}{\tau_n} + \frac{G(N_0 - N_t)S}{(1+\epsilon S)} \tag{2}$$

where N_0 is the carrier number, S is the photon number, N_t is transparency carrier density, η_i is the current injection efficiency, β is the spontaneous emis-

sion factor, ϵ is the gain saturation factor and I_l is the leakage current. Carrier lifetime and photon lifetime are τ_n and τ_p respectively.

We model the instantaneous wavelength of the VCSEL using the equation given in [1].

$$\lambda(t) = \lambda_0(1 - \frac{\rho(N_0 - N_t)}{n} + \frac{dn}{dT}\frac{(T - T_0)}{n}) \tag{3}$$

The instantaneous wavelength depends on carrier number and temperature. T_0 is the ambient temperature, ρ is the refractive index change per unit carrier number change and n is the refractive index of the medium. Fig. 1 shows a comparison of the experimental and simulated L-I characteristics for a single mode Honeywell VCSEL SV3639. Simulated results agree well with the experimental results over a range of temperature.

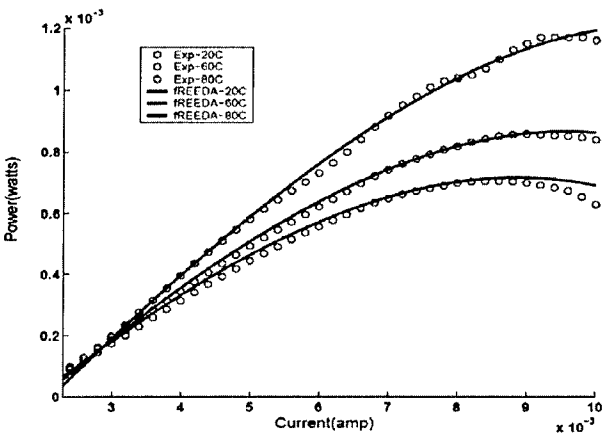

Fig. 1. Experimental and simulated L-I curves for VCSEL at different temperatures.

We also used the L-I and I-V characteristics from the CFDRC physical VCSEL model to extract the VCSEL parameters. Fig 2. shows the CFDRC VCSEL model along with the parameter extraction procedure. Simulated L-I and I-V characteristics are compared with the CFDRC VCSEL L-I and I-V characteristics in fig. 3a and fig. 3b respectively. There is a good agreement between the simulated and the CFDRC physical VCSEL characteristics.

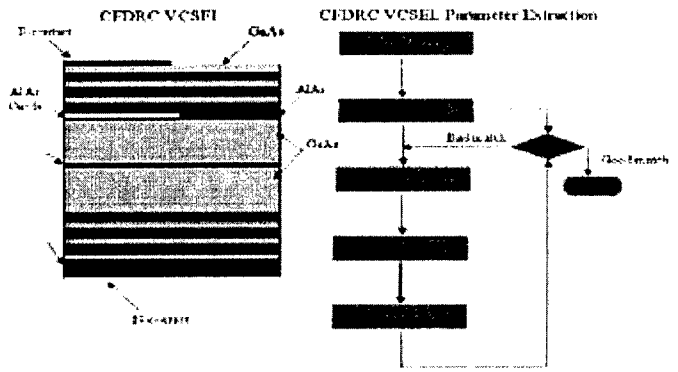

Fig. 2. CFDRC VCSEL physical model and parameter extraction procedure.

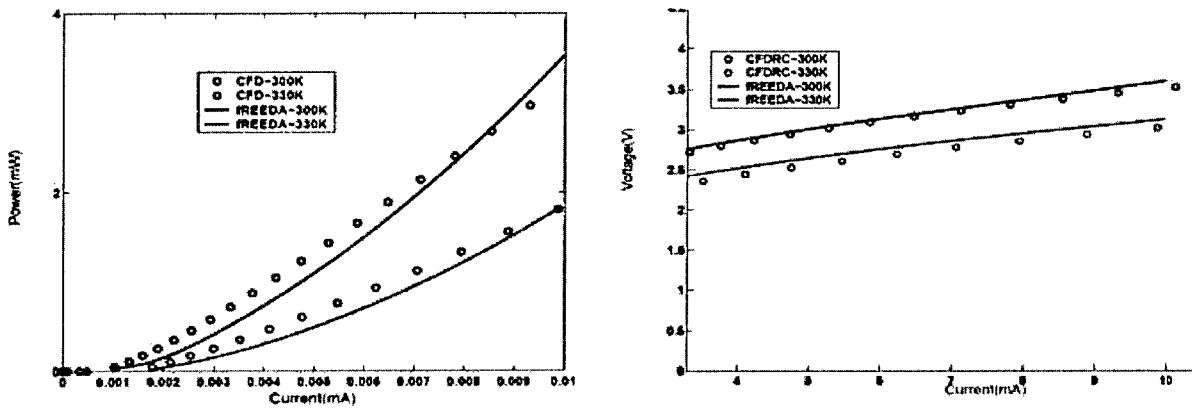

(a) (b)

Fig. 3. Comparison of the CFDRC VCSEL characteristics with the fREEDA results using extracted parameters . (a) L-I characteristics at different temperatures . (b) I-V characteristics at different temperatures.

We also did a study of the electrical interactions that take place in the packages connecting the VCSEL array to the VCSEL driver array [1]. fREEDA package results are compared with the SPICE results in figures 4,5 and 6. Fig. 4 and 5 show a comparison of output optical power from fREEDA and SPICE for a thin-film package at 1GBps and 2.5 GBps respectively. A comparison of the output optical power for a flip-chip package at 5GBps is presented in fig. 6.

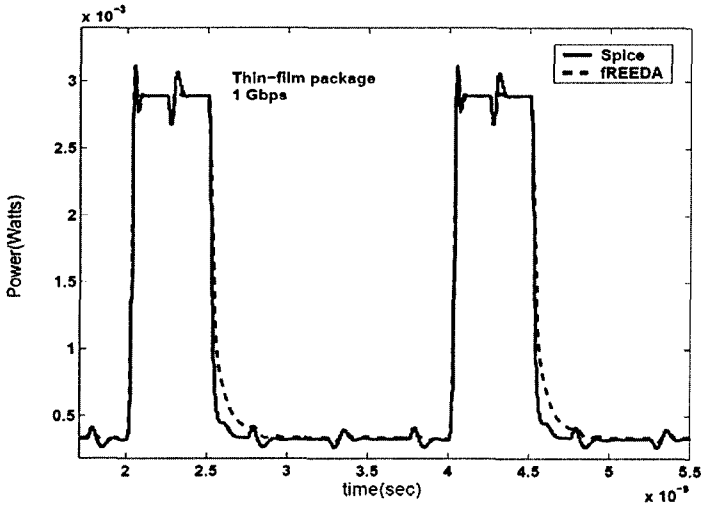

Fig. 4. Comparison of fREEDA and SPICE results for thin-film package at 1GBps.

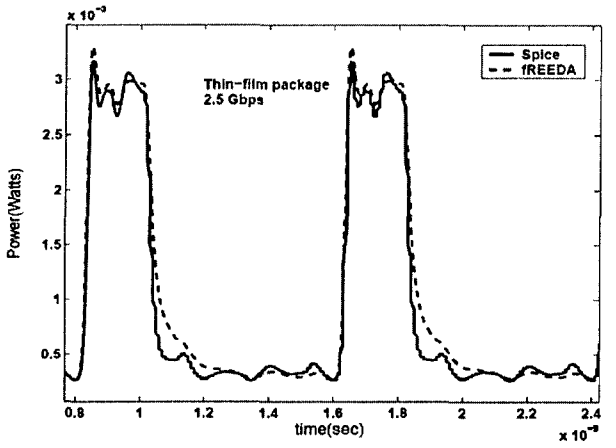

Fig. 5. Comparison of fREEDA and SPICE results for thin-film package at 2.5GBps.

Details of the packages used in simulations are given in [1].

4.3 Multimode VCSEL Modeling

Next we present the simulation results for a multimode VCSEL. We modeled the multimode VCSEL using the model described in [2]. Following equations

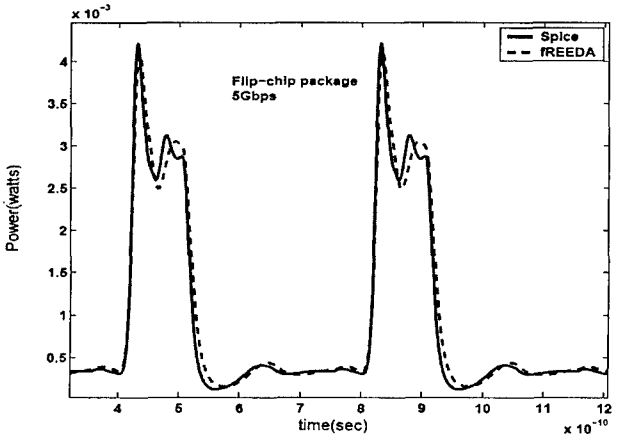

Fig. 6. Comparison of fREEDA and SPICE results for flip-chip package at 5GBps.

were used in our simulations:

$$\frac{dN_0}{dt} = \frac{\eta_i I}{q} - \frac{N_0}{\tau_n} - \sum_k \frac{G(\gamma_{k0}N_0 - \sum_i \gamma_{ki}N_i - \gamma_{k0}N_t)S_k}{(1+\sum_m \epsilon_{mk}S_m)} - \frac{I_l}{q} \quad (4)$$

$$\frac{dN_j}{dt} = -\frac{\eta_i I}{q}\zeta_j - \frac{N_j}{\tau_n}(1+h_j) + \sum_k \frac{G(\phi_{jk0}N_0 - \sum_i \phi_{jki}N_i - \phi_{jk0}N_t)S_k}{(1+\sum_m \epsilon_{mk}S_m)} \quad (5)$$

$$\frac{dS_k}{dt} = -\frac{S_k}{\tau_{pk}} + \frac{\beta_k}{\tau_n}[b_0N_0 - \sum_i b_iN_i] + \sum_k \frac{G(\lambda_{k0}N_0 - \sum_i \lambda_{ki}N_i - \lambda_{k0}N_t)S_k}{(1+\sum_m \epsilon_{mk}S_m)} \quad (6)$$

These spatially independent rate equations are derived and explained in [2]. Though, these equations are spatially independent they very well capture the spatial effects, such as spatial hole burning, required for multimode operation through N_1. We represent the DC and transient results for a two mode VCSEL. Fig. 7 shows the L-I characteristics for a two mode VCSEL. From fig. 7 it is clear that the threshold for mode 2 is higher than that for mode 1 since the emission of mode 2 require a spatial hole to burn which occurs at higher current. Once a spatial hole is burned, the carrier profile changes to support the emission of LP_{11} mode. A kink appear in the L-I characteristics of LP_{01} mode at the point where LP_{11} mode begins to lase, changing the slope of the L-I curve for LP_{01} mode.

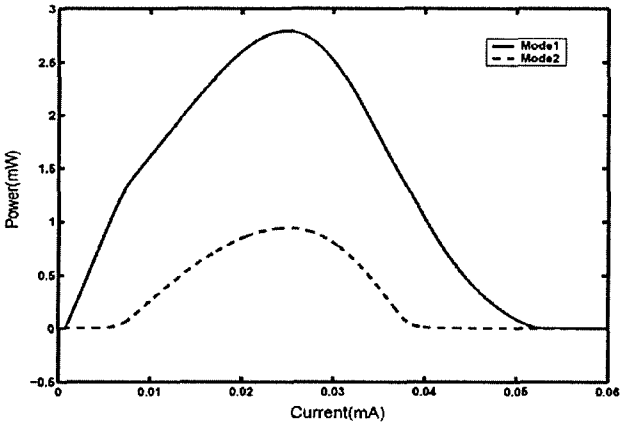

Fig. 7. L-I characteristics for a multimode VCSEL. Continuous line shows LP_{01} mode and dashed line shows LP_{11} mode.

Transient results for a two mode VCSEL are shown in figure 8. Here also we see that the mode 2 start lasing at a later instant, showing the importance of SHB in the emission of LP_{11} mode. Once the output of mode 1 goes down it comes up again which is seen as a little bump in the LP_{01} power output. These secondary pulsations occur due to the diffusion of carriers towards the spatial hole once the device is switched off. These results show the capability of fREEDA in simulating the complex spatial behavior of a multimode VCSEL using the system of equations. To simulate the similar behavior in other circuit simulators one need to generate an equivalent circuit corresponding to these equations. Further, different circuit models for different types of analysis, such as DC, transient and AC, are required in other circuit simulators, whereas any type of analysis can be performed in fREEDA using the same set of equations.

4.4 Free Space Propagation

This section discusses the modeling of a free space optical system using fREEDA. We model the free space propagation using the gaussian beam propagation

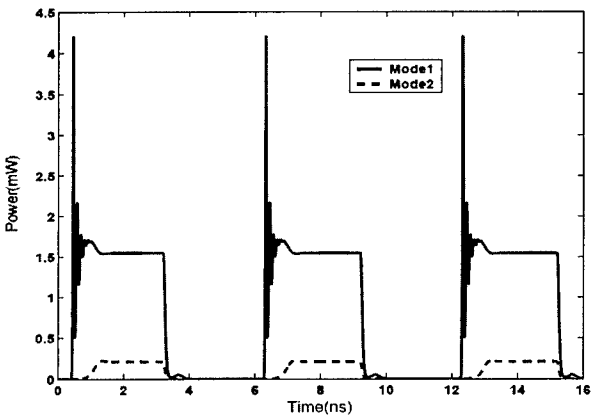

Fig. 8. Transient characteristics for a multimode VCSEL. Continuous line shows LP_{01} mode and dashed line shows LP_{11} mode.

model. For gaussian propagation the beam width at a distance z is given by:

$$w(z) = w_0\sqrt{1 + (z/z_r)^2} \tag{7}$$

where w_0 is the beam waist size, z_r is the rayleigh range. Rayleigh range z_r is related to the wavelength λ and the beam waist w_0 by the following equation:

$$z_r = \pi w_0^2/\lambda \tag{8}$$

Fig. 9 shows a simple free space optical system imaging an input beam to output beam using a lens.

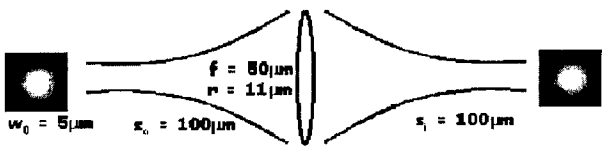

Fig. 9. System diagram for free space gaussian propagation.

However, finite size of the lenses and other apertures clip the beam leading to power reduction and diffraction effects[3]. Power reduction caused by the finite circular aperture can be modeled using equation:

$$P_{new} = P(1 - \exp(-2k^2)) \tag{9}$$

where k = D_{apt}/w_{apt}, is the ratio of the aperture diameter to the spot size at the aperture input. Presence of the aperture modifies the beam width to:

$$w_{aapt} = w_0(1 - \exp(-2k^2).cos(pk^2/(2\pi))) \tag{10}$$

and the new rayleigh range to:

$$z_{ar} = \pi w_{aapt}^2/\lambda \tag{11}$$

where p = $2\pi(z/z_r)$, z_r is the initial rayleigh range and z represent the distance from waist to the aperture. We imaged a laser beam of spot size $w_0 = 5\mu$m using a lens of focal length f = 50μm. The laser was placed at 100μm and the spot size and power was detected at 100μm. To observe the effect of clipping we varied the lens diameter from 10μm to 33μm. Fig. 10 and 11. show the effect of clipping on detected spot size and power. Detected power and spot size did not show any change for an aperture diameter of 33μm. But as the aperture size is reduced further, spot size increases due to diffraction leading to reduced detected power.

Fig. 10. Effect of lens aperture size on spot diagram at detector plane.

We also modeled the free space propagation using the following ray tracing equations:

$$Q = Hcos(U) - usin(U) \tag{12}$$

$$sin(I) = Q/R_1 + sin(U) \tag{13}$$

$$sin(I_1) = nsin(I)/n_1 \tag{14}$$

$$U_1 = U - I + I_1 \tag{15}$$

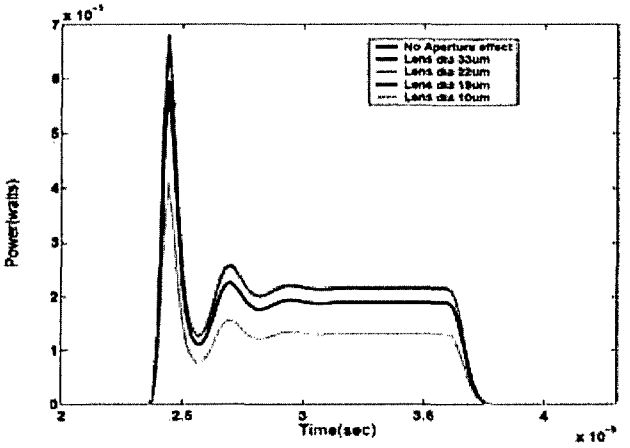

Fig. 11. Detector power for different lens aperture sizes showing reduction in detected power as the lens aperture is reduced.

$$Q_1 = Q(cos(U_1) + cos(I_1))/(cos(U) + cos(I)) \tag{16}$$

where Q is the distance from the vertex of the surface to the incident ray and perpendicular to the ray. Q_1 is the distance from the vertex of the surface to the refracted ray and perpendicular to the ray, H is the input ray height, U is the input ray angle, I is the angle of incidence, I_1 angle of refraction and u object distance.

Ray tracing is good for the first order optical design as it brings out the aberrations present in the system. Figures 12a and 12b show the effect of plano-convex lens on the spherical aberration. We see that spherical aberration is more when plane surface is placed towards the source, which is usually the case. Presence of field curvature is shown in fig. 13.

The effects of aberrations and diffraction can be reduced at an early stage of design by choosing the lenses corrected for aberration and with large aperture. But problems can still arise due to the presence of dispersive elements. When a laser is directly modulated it gives rise to the ringing noise and wavelength chirp [1]. Fig. 14 shows a system having a diffraction grating as a dispersive element. Because of the wavelength chirp, the grating causes a temporal

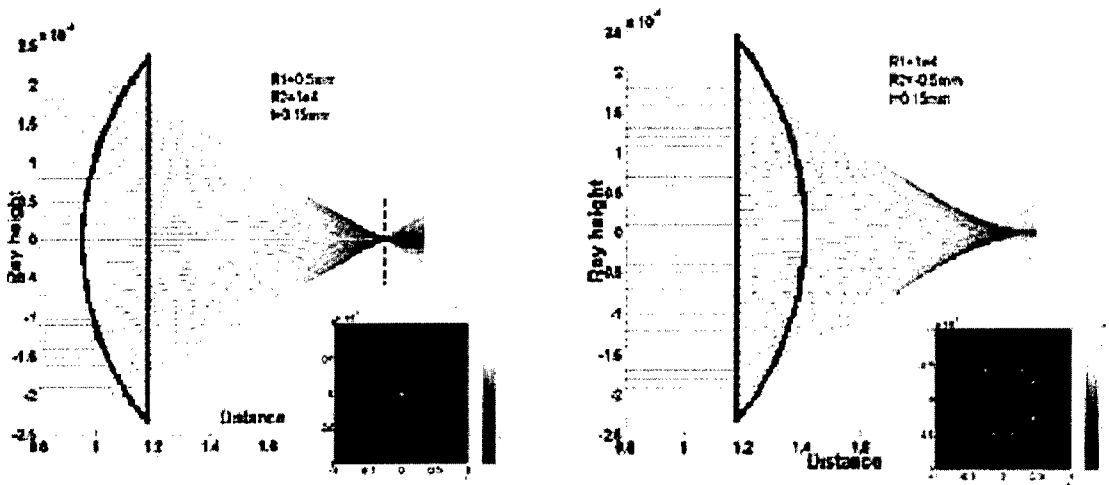

(a) (b)

Fig. 12. Ray trace diagram for plano-convex lens. (a) With convex surface towards the source. (b) With plane surface towards the source.

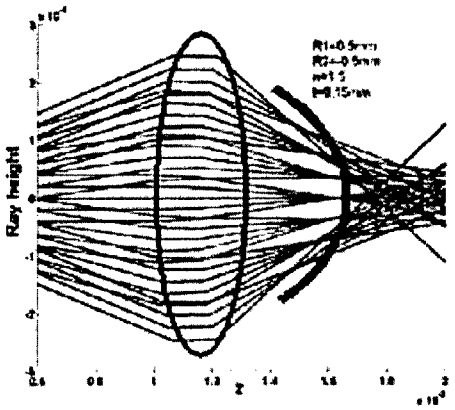

Fig. 13. Ray trace for a binconvex lens showing field curvature.

variation in the beam position on the detector plane as shown in fig 15.

This temporal variation in the position on the detector plane gives rise to detector crosstalk in a free space optical interconnect(FSOI). Fig. 16 shows the spot size on different detector positions as a function of time. Optical

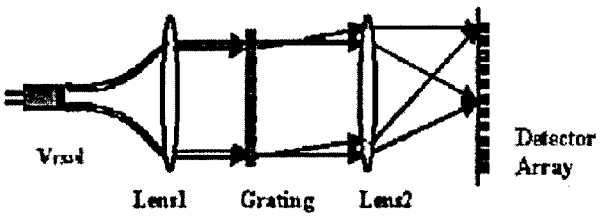

Fig. 14. System diagram for grating spectrometer.

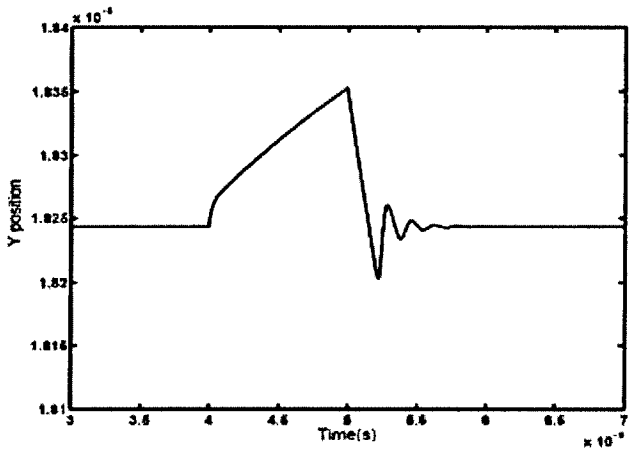

Fig. 15. Variation of spot position on detector array plane.

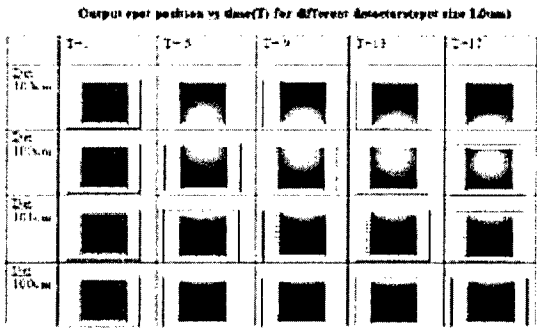

Fig. 16. Spot diagram for variation of spot position on detector array with time.

power measured by these detectors is shown in fig. 17.

However, wavelength chirp can be eliminated using external modulation. Fig. 18 shows an electro-optic modulator, where the application of externally applied voltage causes a phase shift between the field in two arms of a Mach-

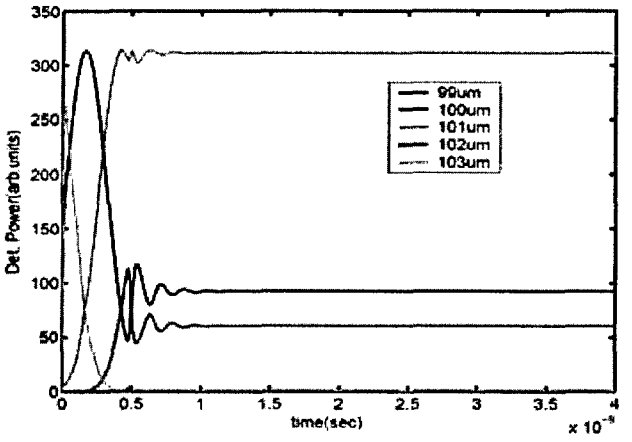

Fig. 17. Output optical power vs. time for different detectors in the detector array.

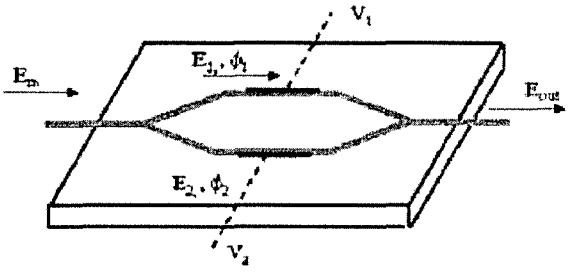

Fig. 18. A simple Electro-optic modulator for external modulation.

Zehnder interferometer. The output of a Mach-Zehnder modulator can be expressed in terms of the applied voltage using the following equation:

$$I_{out} = I_m(\cos(\pi V/(2 * V_\pi)))^2 \tag{17}$$

where I_{out} is the output intensity, I_{in} is the input intensity, V_π is the voltage required for π phase shift and V is the applied voltage.

Fig. 19a and 19b shows the output optical power and wavelength with and without the external modulation. Optical power and the wavelength for the direct modulation case shows ringing and chirp but the external modulation reduces it.

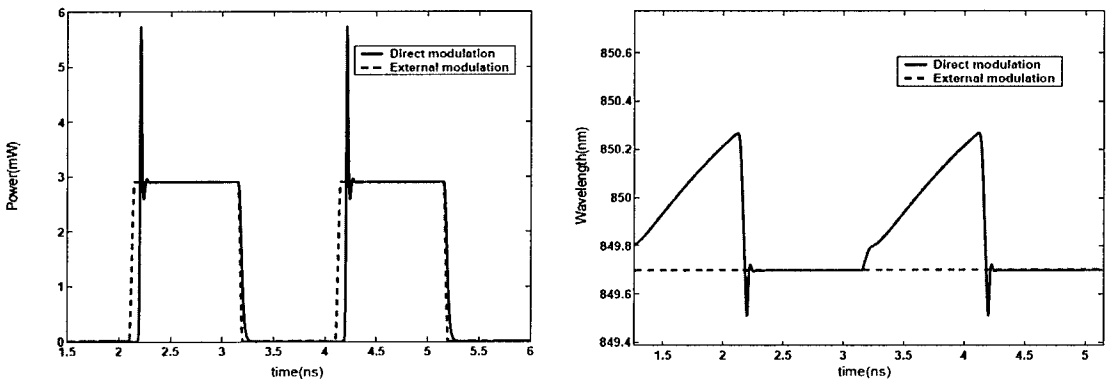

(a) (b)

Fig. 19. Comparison of external and direct modulation. (a) Output optical for direct and external modulation. (b) Wavelength vs. time for direct and external modulation.

The impact of external modulation is more clear from the eye diagrams shown in fig. 20a and 20b. Fig. 20a shows that the eye opening is less in case of direct modulation due to the ringing noise, whereas, the external modulation shows a good eye opening in fig. 20b. Further, use of the external modulation eliminate the detector crosstalk that occurs in the presence of chirp. Spot position on the detector plane is compared for the direct and external modulation in fig. 21 as a function of time. For external modulation, the spot position does not change with time, whereas, for the direct modulation spot position jumps from one detector to another with time.

Thus, fREEDA enables modeling and design of optical systems using the simple set of equations. To perform a similar system study using other circuit simulators, require converting each and every equation into an equivalent circuit [4]. We see that one can study the various interactions that take place in a system using fREEDA but the most unique feature of fREEDA is its ability to make the optical feedback study possible. fREEDA has a delay element that makes it possible to take into account the reflection from each optical surface back to the laser source. Next section is devoted to optical feedback

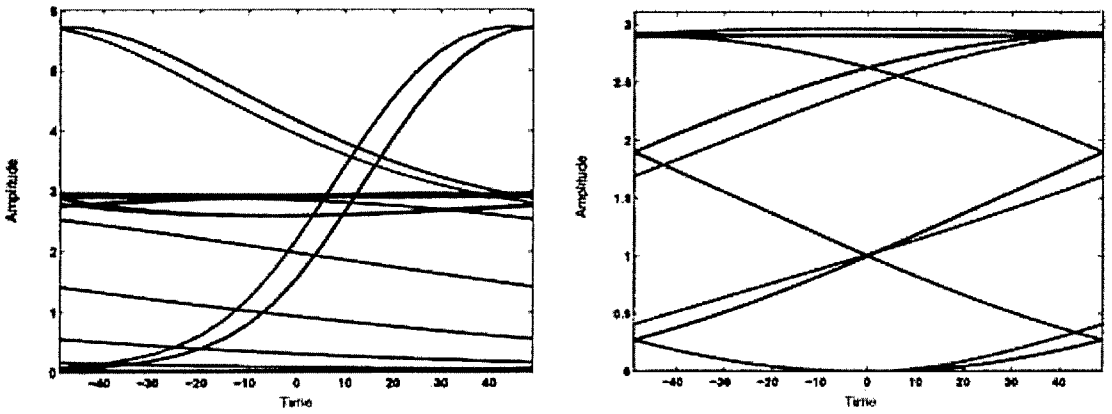

(a) (b)

Fig. 20. Comparison of eyediagrams for external and direct modulation. (a) Eye diagram for direct modulation shows less eye opening. (b) Eye diagram for external modulation show good eye opening.

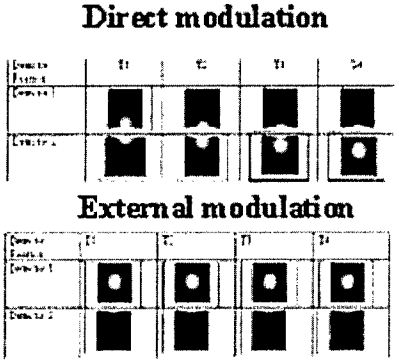

Fig. 21. Comparison of spot diagrams on detector plane for direct and external modulation.

study using fREEDA.

4.5 Optical Feedback Study

Optical feedback plays an important role in optical communication systems. Even a small amount of feedback can cause instability in the laser output resulting in system performance degradation. But, one can also use optical

feedback for useful applications e.g. strong feedback can give rise to single mode operation and line narrowing. So, one should consider reflection from optical surfaces while designing an optical system. We model the feedback using Lang-Kobayashi equations [5].

$$\frac{dN_0}{dt} = \frac{\eta_i I}{q} - \frac{N_0}{\tau_n} - \frac{G(N_0 - N_t)S}{(1+\epsilon S)} - \frac{I_l}{q} \tag{18}$$

$$\frac{dS}{dt} = -\frac{S}{\tau_p} + \frac{\beta N_0}{\tau_n} + \frac{G(N_0 - N_t)S}{(1+\epsilon S)} + 2\kappa\sqrt{S(t)S(t-\tau)}cos(w_0\tau + \eta t) \tag{19}$$

$$\frac{d\phi}{dt} = -(w_0 - w_{th}) + \alpha\frac{G(N_0 - N_t)S}{2(1+\epsilon S)} - \kappa\sqrt{S(t-\tau)/S(t)}sin(w_0\tau + \eta t) \tag{20}$$

Where $\tau = 2L_{cxt}/c$ is the round trip time of external cavity, $\kappa = \frac{(1-R)}{\tau_L}\sqrt{R_{ext}/R}$, R_{ext} is the reflectivity of external reflector, R is the reflectivity of laser mirror and τ_L is the round trip time of internal cavity. Optical feedback has been studied extensively by various groups and five regimes of feedback have been identified. Fig. 22 show various regimes of optical feedback. Fig. 22 has the output optical power and the corresponding phase plots. We see that the output optical power approaches stable point for low reflectivity and short distance. As the distance and reflectivity is increased, output power exhibit a limit cycle followed by chaotic output.

To our knowledge none of the groups have studied the impact of the optical feedback on system performance. Here, we discuss the impact of the optical feedback on system performance. Fig. 23 shows an imaging system, with optical feedback from different reflective surfaces. We calculate the resultant field at each surface and then propagate it back to the laser.

In our study, we consider the reflection from single lens and two lens system. The output optical power and output wavelength for these two systems are shown in fig. 24 and fig. 25.

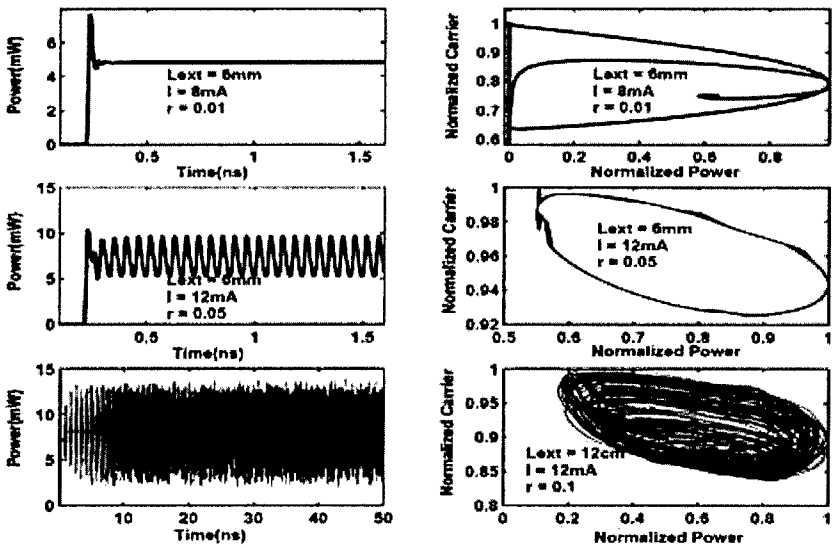

Fig. 22. Different regimes of optical feedback.

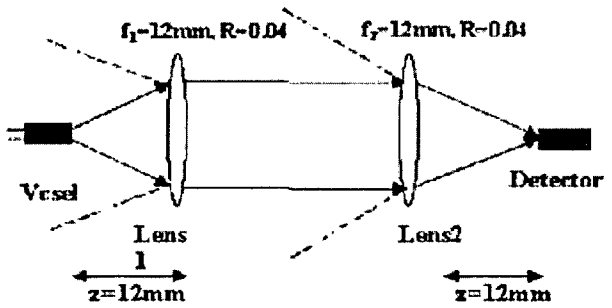

Fig. 23. Two lens system depicting optical feedback from different components.

We see that the optical power and wavelength show instability confirming that even a small amount of feedback can degrade the system performance. In previous section, we saw that by using the external modulation one can eliminate the chirp and improve eye opening but there we didn't consider the effect of feedback. To see how optical feedback impact the system performance, we consider the grating spectrometer system shown in fig. 14 and looked at the output optical power on a fixed detector in the detector array as shown in fig. 26.

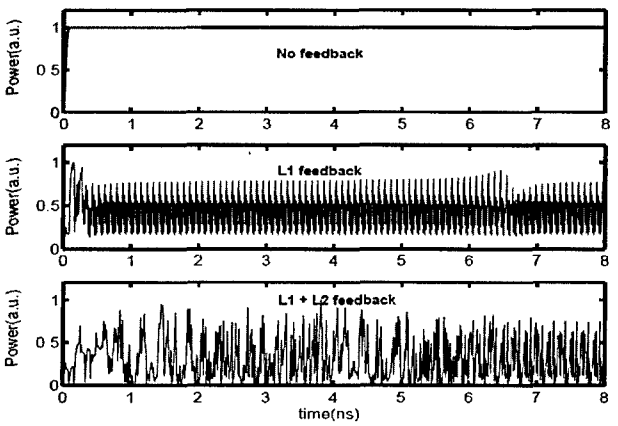

Fig. 24. Effect of optical feedback on output optical power in a single lens and two lens system.

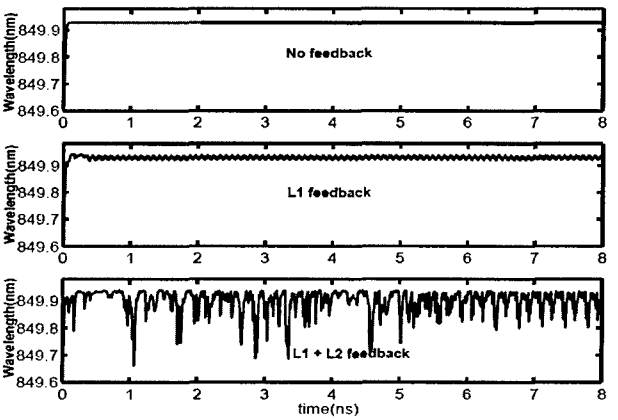

Fig. 25. Effect of optical feedback on output wavelength in a single lens and two lens system.

The output optical power varies randomly with time on the detector because of instability in wavelength. If there had been no feedback and we were using the external modulation, then the output spot should have stayed at one detector as shown in fig 21. Fig. 26 shows the output optical power on a fixed detector for no feedback, feedback from a single lens and feedback from two lenses.

Further, we noticed that for small feedback and small distance, within coherence length of laser output, output power shows a sinusoidal behavior with period equal to half the wavelength. We also noticed that the feedback causes

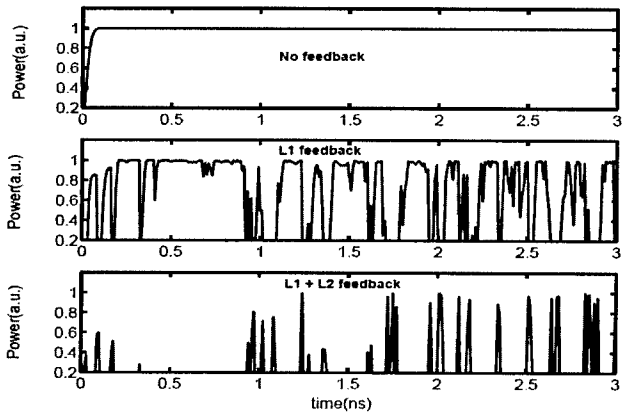

Fig. 26. Effect of feedback on detector output for single lens and two lens system.

a change in the terminal voltage. Fig. 27 shows a plot of voltage vs. reflectivity. The terminal voltage reduces as we increase the reflectivity because increased reflectivity causes more charge carriers resulting in reduced input impedance and thus, the voltage. One can utilize this variation in voltage with feedback for making compact imaging or readout systems [7,8]. The change in the input impedance with optical feedback can cause impedance mismatch between the laser driver output and the laser input causing signal reflections, effecting system performance. Thus, feedback can be fatal if not properly taken into consideration while designing the system. So, the study suggest that any system design must take feedback into account which indirectly implies that the tool used for design should be capable of including feedback in system design.

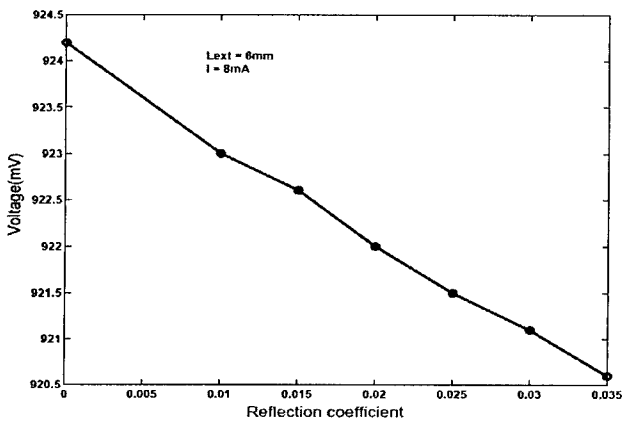

Fig. 27. Effect of increasing feedback on terminal voltage of laser.

4.6 Conclusion

We present a study of free space optical system using fREEDA, Our results demonstrate its capabilities in understanding the interactions that can effect the system performance under different scenarios. fREEDA can easily implement any complex device such as multi-mode VCSEL using simple set of equations, whereas same device modeling in other circuit simulator would require converting these equations into equivalent circuit. fREEDA can also capture the impact of optical feedback in system performance. Results show that one can design a full system using simple equations and understand the performance related issues before actually fabricating the system.

References

[1] Ravi Pant, Mark A. Neifeld, Michael B. Steer, Houssam Kanj, and Andreas Cangellaris *Optics Communications* (2004).

[2] Pablo V.Mena, J.J.Morikuni, S.M.Kang, A.V.Harton, and K.W.Wyatt *J. Lightwave Technol.* **17** (1999), p.865.

[3] S.P.Levitan, P.J.Marchand, T.P.Kurzweg, M.A.Rempel, D.M. Chiarulli, C.Fan, and F.B.McCormick *Proceedings of the 34th IEEE/ACM Design Automation Conference*, Anaheim CA (1997).

[4] Mark A. Neifeld and Wu-Chun Chou, *Applied Optics* **37** (1998).

[5] Land and Kobayashi, *Int. Journal of RF and Microwave Computer-Aided Engineering* **9** (1999), p. 376.

[6] C.E.Christoffersen, U.A.Mughal and M.B.Steer, *Int. Journal of RF and Microwave Computer-Aided Engineering,* **10** 2000, p. 164.

[7] Aditya kalavguta and Mark A. Neifeld *OSA annual meeting 2003.*

[8] Jiro Hashizume, Satoshi Shinada, Fumio Koyama and Kenichi Iga*Microsystem Research Center, P I Lab, Tokyo Institue of Technology.*

[9] M. S. Basel, M. B. Steer and P. D. Franzon, "Simulation of high speed interconnects using a convolution-based hierarchical packaging simulator," *IEEE Trans. on Components, Packaging, and Manufacturing Techn.*, 18 February (1995) 74.

[10] W. Batty, C. E. Christoffersen, A. B. Yakovlev, J. F. Whitaker, M. Ozkar, S. Ortiz, A. Mortazawi, R. Reano, K. Yang, L. P. B. Katehi, C. M. Snowden and M. B. Steer, "Global coupled EM-electrical-thermal simulation and experimental validation for a spatial power combining MMIC array," *IEEE Trans. Microwave Theory and Techn.*, Dec. (2002) 2820.

5. Publications

5.1 Papers directly supported by the DARPA NeoCAD Project

1. R. Pant, M. A. Neifeld, M. B. Steer, H. Kanj, and A. C. Cangellaris, "Electrical package impact on VCSEL-based optical interconnects," submitted to *Optics Communication*, October 2004.
2. A. Varma, M. Steer, P. Franzon, "SSN issues with IBIS models," *Electrical Performance of Electronic Packaging*, October 2004.
3. S. Luniya, M. B. Steer and C. E. Christoffersen, "High dynamic range transient simulation of microwave circuits," *IEEE Radio and Wireless Conf. (RAWCON)*, 2004.
4. F. Hart, N. Kriplani, S. Luniya, C. Christoffersen and M. B. Steer "Streamlined circuit device model development with fREEDA and Adol-C," *AD 2004 — Fourth International Workshop on Automatic Differentiation*, July 2004.
5. R. Mohan, J. C. Myoung, S. E. Mick, F. P. Hart, K. Chandrasekar, A. C. Cangellaris, P. D. Franzon and M. B. Steer, "Causal reduced-order modeling of distributed structures in a transient circuit simulator," *IEEE Transactions on Microwave Theory and Techiques*, Vol. 52, September 2004, pp. 2207–2214.
6. V. I. Okhmatovski, J. D. Morsey, A. C. Cangellaris, "Loop-tree implementation of the adaptive integral method (AIM) for numerically-stable, broadband, fast electromagnetic modeling," *IEEE Transactions on Antennas and Propagation*, Vol. 52, August 2004.
7. J. C. Myoung, S. E. Mick, F. P. Hart, K. Chandrasekar, A. C. Cangellaris "Comprehensive broadband EM modeling of on-chip interconnects with surface discretization-based generalized PEEC model," in review.
8. V. I. Okhmataovski, A. C. Cangellaris, "Evaluation of layered media green's functions via rational function fitting," *IEEE Microwave and Wireless Components Letters*, Vol. 14, January 2004.
9. V. I. Okhmatovski, J. D. Morsey, A. C. Cangellaris, "Enhancement of the numerical stability of the adaptive integral method at low frequencies through a loop-charge formulation of the method-of-moments approximation," *IEEE Transaction on Microwave Theory and Techniques*, Vol. 52, March 2004.
10. J. D. Morsey, V. I. Okhmatovski, A. C. Cangellaris, "Finite-thickness conductor models for full-wave analysis of interconnects with a fast integral equation method," *IEEE Transactions on Advanced Packaging*, Vol. 27, February 2004.
11. V. I. Okhmatovski, J. D. Morsey, A. C. Cangellaris, "On deembedding of port discontinuities in full-wave CAD models of multiport circuits," *IEEE Transactions on Microwave Theory and Techniques*, Vol. 51, December 2003.
12. A. Rong, A. C. Cangellaris, L. Dong, "A novel effective surface impedance formulation for efficient broadband modeling of lossy thick strip conductors," in review